NISTIR 89-4040

High-Current Measurement Techniques, Part II 100-kA Source Characteristics and Preliminary Shunt and Rogowski Coil Evaluations

J. D. Ramboz

U.S. DEPARTMENT OF COMMERCE
National Institute of Standards and Technology
(Formerly National Bureau of Standards)
National Engineering Laboratory
Center for Electronics and Electrical Engineering
Electricity Division
Gaithersburg, MD 20899

March 1989

Sponsored by:
Sandia National Laboratories
Albuquerque, New Mexico

NISTIR 89-4040

High-Current Measurement Techniques, Part II 100-kA Source Characteristics and Preliminary Shunt and Rogowski Coil Evaluations

J. D. Ramboz

U.S. DEPARTMENT OF COMMERCE
National Institute of Standards and Technology
(Formerly National Bureau of Standards)
National Engineering Laboratory
Center for Electronics and Electrical Engineering
Electricity Division
Gaithersburg, MD 20899

March 1989

National Bureau of Standards became the National Institute of Standards and Technology on August 23, 1988, when the Omnibus Trade and Competitiveness Act was signed. NIST retains all NBS functions. Its new programs will encourage improved use of technology by U.S. industry.

Sponsored by:
Sandia National Laboratories
Albuquerque, New Mexico

U.S. DEPARTMENT OF COMMERCE
Robert A. Mosbacher, Secretary
Ernest Ambler, Acting Under Secretary for Technology
NATIONAL INSTITUTE OF STANDARDS AND TECHNOLOGY
Raymond G. Kammer, Acting Director

TABLE OF CONTENTS

LIST OF FIGURES

HIGH-CURRENT MEASUREMENT TECHNIQUES, PART II
100-kA SOURCE CHARACTERISTICS AND PRELIMINARY SHUNT AND ROGOWSKI COIL EVALUATIONS

J.D. Ramboz

Abstract

The characterization of a 100-kA current source is discussed. This source is intended for use in the calibration of high-current sensors such as shunts and Rogowski coils commonly employed in resistance welders. The output current from the source is in the form of bursts of "chopped" 60-Hz sinusoidal waveforms. These waveforms and their spectral content were investigated. The near-field magnetic field strength was mapped. Initial calibrations were performed on a 30-kA, 10-$\mu\Omega$ shunt. Preliminary results indicate a temperature coefficient of about 130 ppm/°C which is thought to be related to a thermally induced strain. Several Rogowski coil type current sensors were evaluated and calibrated. Each of the coils measured had outputs which were sensitive to the rotational position about the current carrying conductor. The calibration philosophy and approach are discussed and estimates of measurement uncertainty are given. Suggested improvements for the measurement process are offered. Planned efforts are outlined.

Keywords: ac current measurements; ac current shunts; calibration; high-current generation; high-current measurements; Rogowski coils

1. INTRODUCTION

The goal of this effort is to study the feasibility of accurate measurement of high currents, up to 100 000 amperes peak, and secondly, to develop methods for the calibration of shunts and Rogowski-coil current sensors, in situ, at the site of resistance welders. The quality and repeatability of critical welding processes can be related to the rms currents used. The currents are gated bursts of 60-Hz sine waves, or portions thereof, depending on the firing angle of control signals and generally have overall durations of tens-of-milliseconds (multiple periods of a 60-Hz wave train). The development of measurement techniques, development of measurement apparatus and devices, and the evaluation of both hardware and software used for the measurement and evaluation of high-pulsed currents are being pursued. For the calibration of the current sensors typically used, an uncertainty of ±1.0% is the ultimate goal. With better calibrations of the current sensors, the cost of maintaining quality control in the welding industry can be reduced.

This report discusses the installation and characterization of a 100-kA current source, initial measurement methods for 30-kA, 10-$\mu\Omega$ shunt calibrations, initial results for the calibration of such shunts using a precision Rogowski coil (mutual inductor) as the reference element, and a short discussion of planned efforts.

The 100-kA current source hardware, circuits, and controller are described. The characterization of the source includes subjects such as the available output current for different control settings, waveform plots as a function of control settings, harmonic content for different settings, and magnetic field measurements in the near-field. Bus-bar configurations are also discussed briefly.

A description of a 30-kA, 10-$\mu\Omega$ shunt is given, leading to the discussion of the calibration philosophy, digitization and software considerations, development of a calibration process, and initial measurement results. The use and characteristics of the mutual inductor (NBSMI) and an accompanying integrating amplifier (NBSIA) are presented.

Efforts for the next phases of the project are given and discussed. Problems which are anticipated are outlined. Suggested improvements in the measurement process are also discussed.

2. 100-kA CURRENT SOURCE, DESCRIPTION AND CAPABILITY

The high pulsed current measurement laboratory is located at the National Institute of Standards and Technology. It was wired and instrumented expressly for developing a capability and gaining an understanding of the problems associated with the generation and measurement of currents on the order of several thousands of amperes and greater, and generally having durations in the tens-of- to hundreds-of- milliseconds.

The current source is a high-current transformer using primary voltage gated by a pair of 2000-A silicon controlled rectifiers (SCR's). Primary power is obtained from a single-phase 480-V, 500-A service, being fed from a high-voltage vault by about 46 meters of 2-0 copper line, and a flexible 5-meter run of 500 Mcm cable. Power is fed to the system through a 500-A circuit breaker, then through a bank of eight adjustable autotransformers which are employed to set the input voltage to the system. The autotransformer output is then fed to the high-current output transformer via a pair of 2000-A SCR's. The firing voltage signals for the SCR's are derived from a microprocessor based controller. Liquid cooling is provided by a self-contained system for the SCR's and the output current transformer. Figure 1 shows a block diagram of the source and fig. 2 is a photograph of the bus-bar arrangement first used with a 30-kA shunt.

2.1 Output Current Characteristics

There are combinations of factors that affect the current available at the secondary of the output transformer. These are highlighted below and further discussed with overall considerations regarding the desired test conditions. Some of them are adjustable, such as the variable autotransformers and the SCR controller settings, and some are inherently fixed in the installations, such as the source impedance feeding the facility and the secondary load impedance.

The major factors affecting the output current are:

- Powerline voltage
- Powerline source impedance

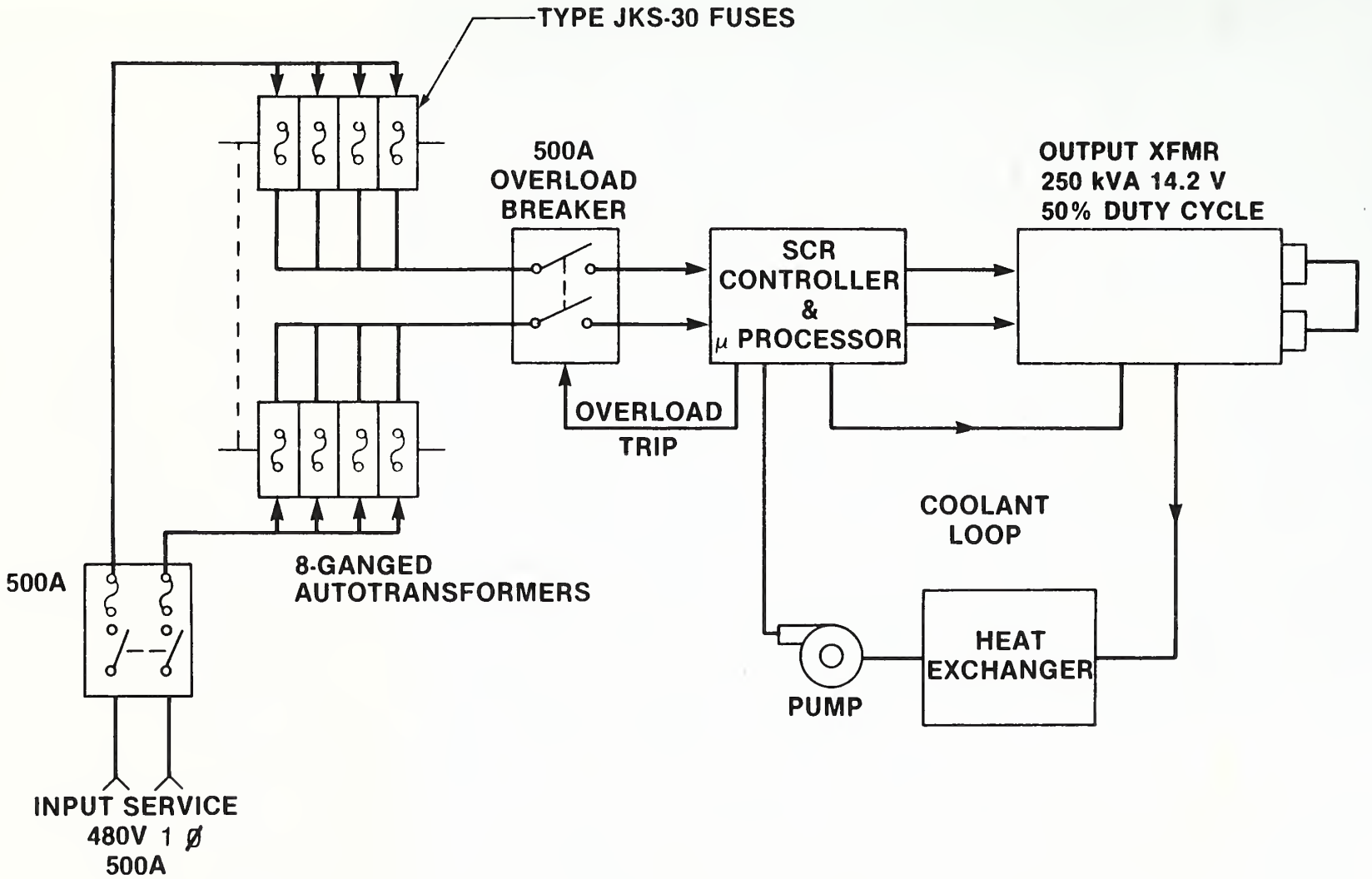

Figure 1. Block diagram of the 100-kA current source. Output current is in the loop to the right of the transformer.

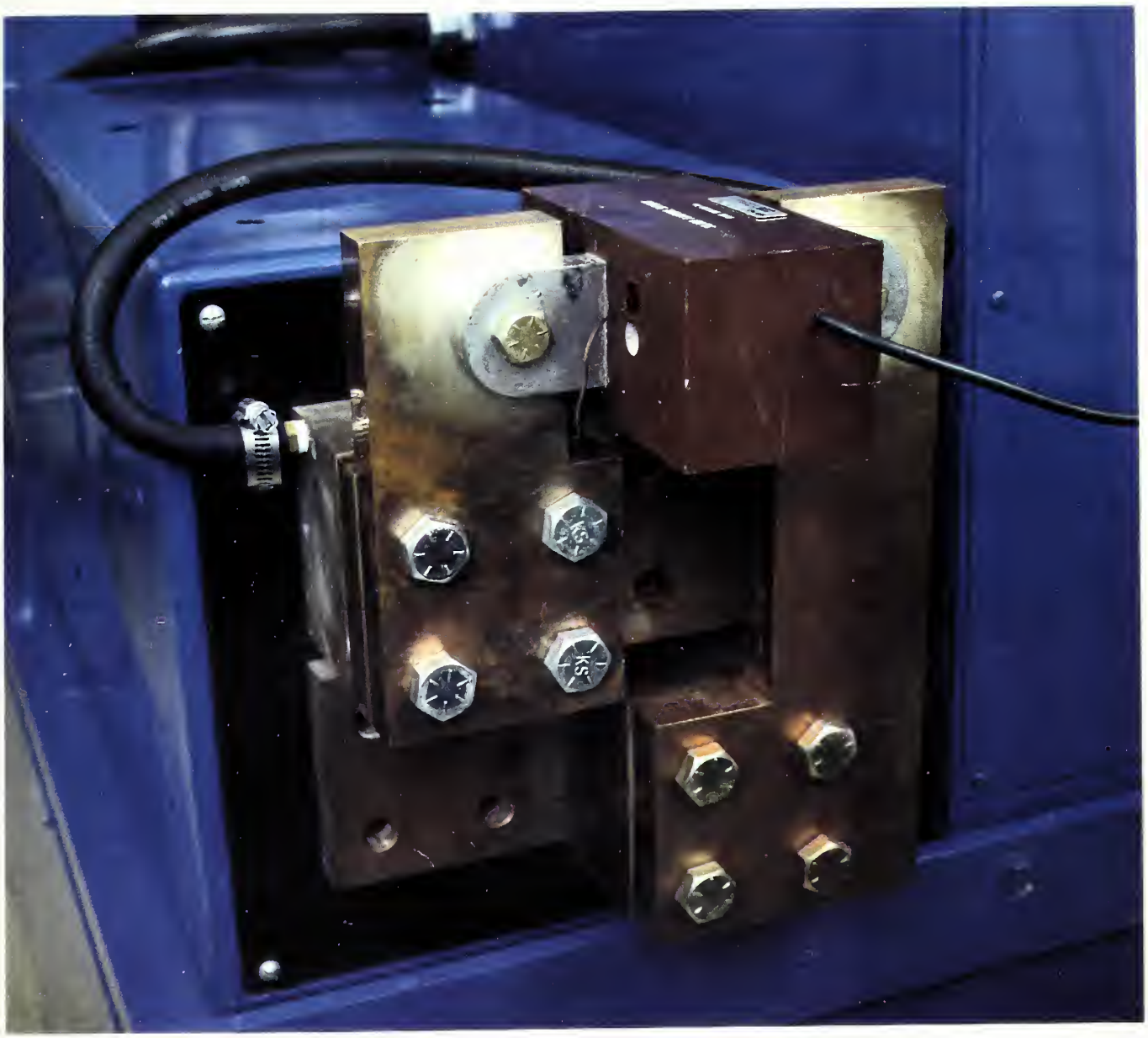

Figure 2. Photograph of the mounting pads and copper bus-bar plates on the output transformer. Also shown is a 30-kA, 10-μΩ shunt. This arrangement presents the minimum useful load impedance to the transformer.

- o Variable autotransformer setting
- o SCR controller settings
  - Number of cycles
  - % heat setting
  - Power factor setting
  - Ramp-up or ramp-down settings
- o Output transformer tap setting
- o Secondary bus-bar and load impedance

Because the powerline supplies the current source, any variations in the line voltage will directly affect the output current. Longer term variations affect the overall value of the peak current at a given transformer setting, and any cycle-to-cycle variation on the powerline will show up as corresponding cycle-to-cycle variations in the output current. At large currents, the primary load on the powerlines is significant, and a voltage drop occurs not only across the feed lines, but also across any other series impedances that are in the system which provides power for the facility. For example, when the source is set to deliver an output current of 100 kA, the powerline sags from a nominal voltage of 480 V to about 416 V and draws about 1000 A from the powerline. Using Ohm's law, the powerline source impedance can be calculated to be about 0.064 ohm. Because of this series impedance, the resulting 64-V drop results in about a 13% decrease in the available output current. At lower than maximum currents, this line drop can be overcome by increasing the autotransformer voltage setting to provide the desired output current. But for the maximum output current, the autotransformers are set to deliver their maximum power (and minimum impedance) and then the controlling factor is the powerline impedance.

The autotransformers consist of eight large, ganged, adjustable transformers arranged in two banks of four devices in parallel. The paralleled transformers use interconnected reactors to balance the current division between transformers. The autotransformers are connected such that their inputs are fed from the single phase 480-V powerline and their output voltage can range from near zero volts to a maximum of about 577 V (120% of the input line).

Figure 3 shows the voltage output (volts rms) from the autotransformers (left-hand ordinate) as a function of the autotransformer dial setting. The voltage ranges from nearly zero volts to a maximum of about 577 V. The output current of the system is plotted against the autotransformer dial setting (right-hand ordinate). The output current ranges from about 10 kA peak as a minimum to a maximum of about 100 kA peak. These values of current were determined by measuring the voltage drop across a 10-$\mu\Omega$ shunt. The controller was set to deliver 4 cycles for a portion of the tests, and 10 cycles for the others. The peak amplitude of the second cycle was arbitrarily used. Table 1 gives the values used for fig. 3.

The lower operating limit is governed by the operation of the SCR's and their inability to function at low voltage levels. This system, as tested and with the particular burden on the output transformer, began developing irregular wave shapes below an output current of about 10 kA because of one SCR failing to conduct continuously. Figure 4 shows a typical waveform for such an instance. Note that the first cycle is completed, but as the automatic power factor logic attempts to adjust the firing angle for the

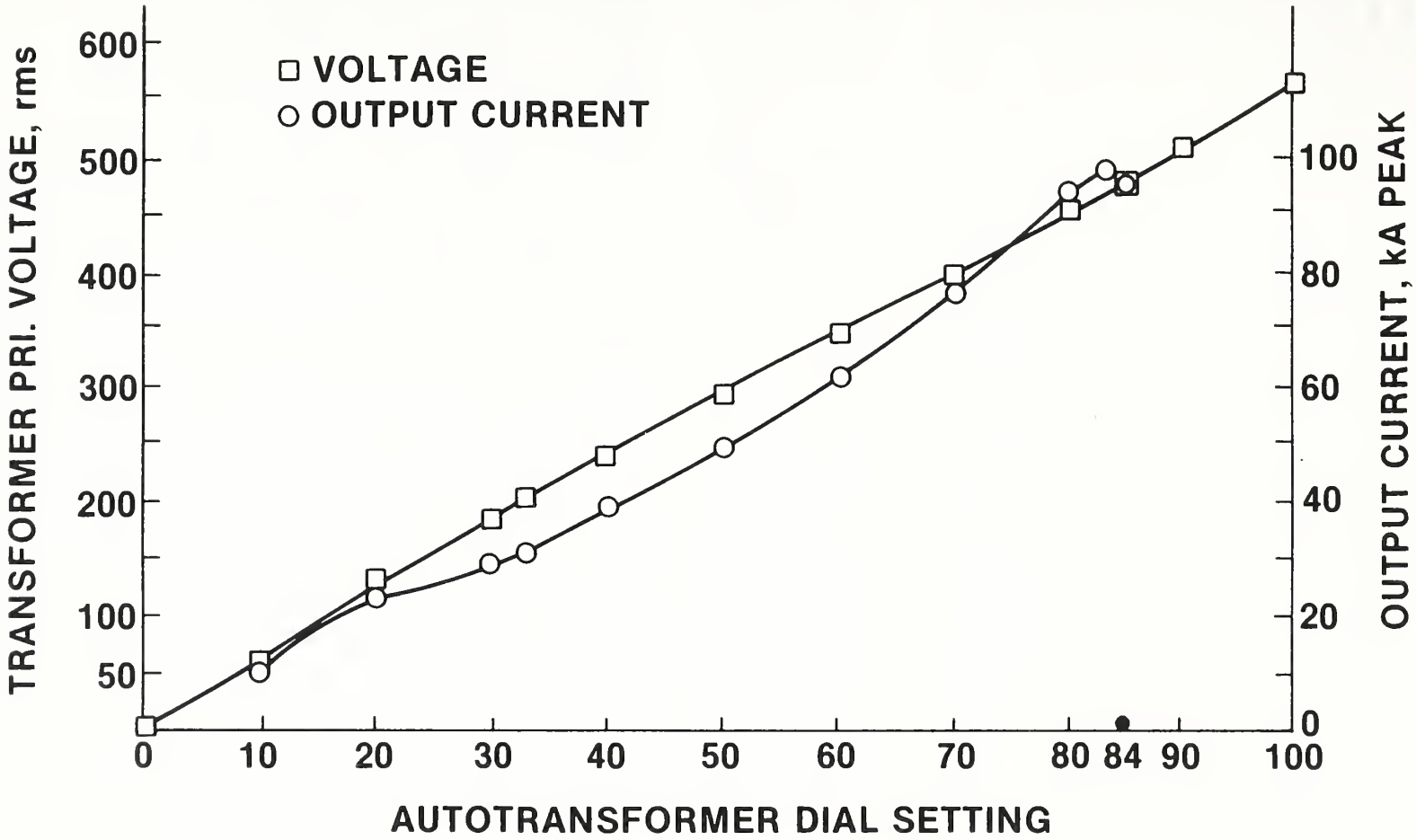

Figure 3. Output transformer primary voltage and secondary current as a function of autotransformer settings.

SCR's, the SCR providing the positive half-cycle fails to conduct for three cycles. It then begins to conduct for the remaining cycles of the 10-cycle burst. When such "clipping" occurs, the output transformer responds by creating an alarmingly loud "thump" sound. (A similar condition can cause SCR malfunction when the automatic power factor feature of the controller is disabled and an improper value of power factor is entered manually.) The ability to disable the automatic feature has certain advantages which will be discussed later, but if an improper value of power factor greater than required is used, especially under more severe loading conditions at very high currents, not only will the output transformer resound loudly when the "clipped" half-cycles are produced, but the system's main circuit breaker will trip off.

Table 1. System voltage and output current as a function of the autotransformer setting.

Autotransformer Setting	Primary Voltage (V, rms)	Output Current (kA, peak)
5	29	----
7.5	43	----
10	59	11.8
15	95	16.6
20	134	25.1
30	188	29.3
33	203	32.2
40	239	39.2
50	293	49.0
60	347	62.2
70	397	77.0
80	458	94.0
84 (dot)	478	98.6
90	506	95.0
100	560	----

The upper output current limit is established by many factors, some of which have been previously discussed or will be discussed in following sections of this report. It is to be noted, however, that under any combination of factors or control settings, the maximum output current will always occur for an autotransformer setting of 84. This is the point where the autotransformer brushes are directly connected to the taps that connect to the 480-V powerlines and represents the minimum series impedance contributions from the autotransformers. Increasing the autotransformer setting does provide more open-circuit, unloaded system voltage, but the high current across the higher autotransformer series impedance creates a larger voltage drop resulting in less current at the output. Note, in fig. 3, how the very upper portion of the output current passes through a maximum value at a

autotransformer setting of 84, then "hooks over" and begins to decrease for higher autotransformer settings.

For the tests described here, the output current maximum was determined by the limits of the fuses for each of the autotransformers. Each autotransformer is individually fused with type JKS-30, 30-A quick acting fuses. At the maximum output current of 100 kA peak, the total powerline current was measured at somewhat greater than 800 A rms which is shared by the eight autotransformers. If the current is divided equally between each of the two groups of four autotransformers, then each 30-A fuse is handling about 100 A rms for four cycles, which for these fuses is their limit. Once the "fusing" temperatures are approached, repeated use continues to fatigue the fuses. The weakest one will blow first, then in quick succession, a number of the rest of them will immediately fail as they each attempt to pickup the total load. As soon as all the four "paralled" fuses in one side or the other of the main powerlines are open, the process stops. When overloaded, at least four fuses must blow, and typically four, five, or six of the eight fuses will blow. If any of the fuses blow, all eight of the 30-A fuses are replaced.

In a separate test, the autotransformers were by-passed to eliminate the effects of their series impedance and the system maximum output current was determined. These tests were also made after the primary 480-V service feeders had been increased in size from 2-0 guage copper to 500 Mcm copper. The load on the output transformer consisted of short flat copper plates with a 10-$\mu\Omega$ shunt connected between them. The increased output current maximum was measured as a 103 kA peak. It was possible to achieve up to 12 cycles of operation before the system circuit breaker tripped. The autotransformers were reconnected and the type JKS-30 quick acting fuses were replaced with type JHC-30 delayed fuses. Tests proceeded by setting the autotransformer to 84 (its lowest impedance setting) and the number of cycles was increased from 3, in steps of one cycle at a time, to determine how many cycles at maximum current the system would tolerate and what limited the overall operation. When 8 cycles were reached, there was a pronounced smell of hot insulation from the autotransformers and testing was halted. The system maximum current capability, when the autotransformers were connected, was established at 103 kA for 8 cycles at 99% heat setting and at a power factor of 0.83. This value does represent the maximum achievable current and operating time, but will, of course, change (probably decrease) for different bus-bar configurations at the output of the high-current transformer.

2.2 Current Waveform Characteristics

The SCR-controller is a microprocessor unit capable of many functions in gating the single-phase voltage which is applied to the primary of the output transformer. Fundamentally, it can be programmed to deliver a preset number of integral periods of a 60-Hz wave train, vary the phase angle of the SCR control signal to provide shorter than half-period current pulses (chopped sine waves), and linear ramp-up or ramp-down control for a preset number of cycles. It also has the ability to sense input line voltage, line-voltage sag, input line current maximum, and determine the power factor of the load. The unit is protected from over current and over temperature conditions. If for some reason the unit trips off, a diagnostic message appears on the controller display the next time the unit is turned on indicating what caused

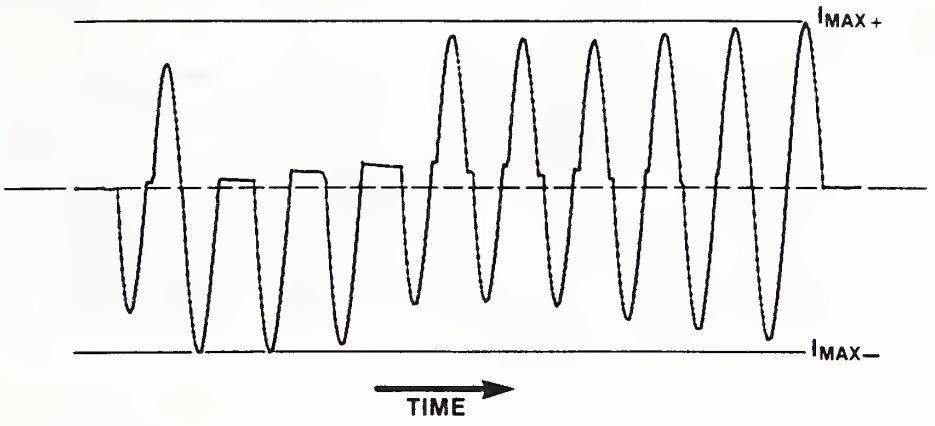

Figure 4. Secondary current "clipping" when one SCR fails to conduct.

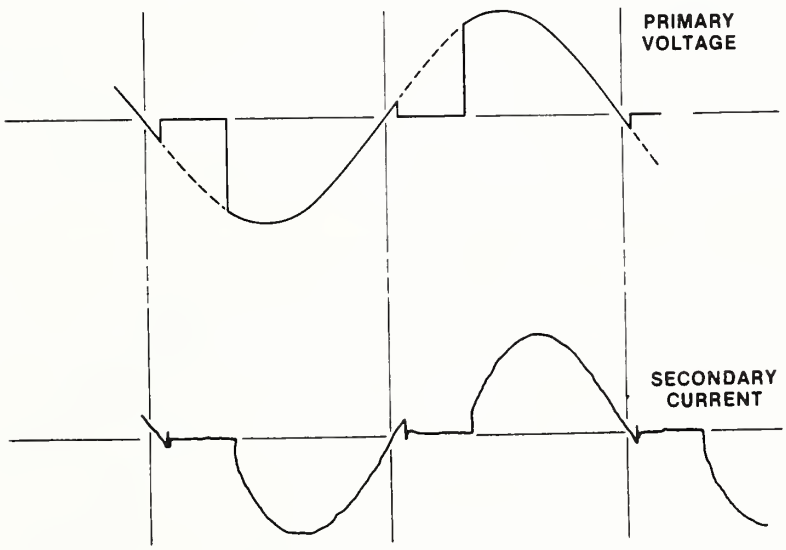

Figure 5. a) Output transformer primary voltage showing SCR controlled "chopping", and b) typical secondary current waveform.

the shut down. The unit is programmable and will retain the program for future use or allow program modifications for different test schedules.

The controller selects the phase (or time delay) for the SCR control signal as a function of the "% heat" which is operator selectable. At a value of 99% heat, the minimum angle is used thus allowing nearly all of the sine-wave voltage to be applied to the primary of the output current transformer. Figure 5a shows a theoretical transformer primary voltage waveform for a heat setting of less than 99%. The SCR conduction does not begin until a portion of the sine wave has occurred at which time the voltage increases in a step-like manner. The voltage waveform then follows the sinusoidal shape until the next zero crossing occurs at which time the SCR conduction ceases. The same operation is repeated during the following half cycle until the programmed number of full cycles has been completed.

The secondary current of the output transformer is shown in fig. 5b. The current waveform is smoothed significantly by the inductive and resistive properties of the transformer and load impedances. It is a LR equivalent circuit and causes the output current always to lag the primary voltage waveform in time. Because each welding system has its individual output transformer properties and load impedance characteristics, the amount of waveform smoothing will be an individual characteristic of each system.

The test results for this portion of the report were obtained using short, flat, two centimeter thick, copper plates to connect to a 10-Ìõ, 30000-A shunt. This presents about the minimum impedance that is practical for the mechanical arrangement of the 250-kVA rated transformer being used. With this arrangement, minimum resistance and inductance are realized, and hence, minimum smoothing of the current waveform occurs. Where similar high-current transformers and controllers are used in welding systems, much larger values of secondary load resistance and inductance will be encountered. Therefore, it is important to maintain a perspective that the waveforms being discussed in this report relate only to this system and apply principally to calibration considerations, and not necessarily to a welding process in other systems. Generally, the increased smoothing that occurs in the secondary current waveform places less stringent requirements on the current measuring instrumentation.

When the automatic power factor feature of the controller is used, the waveform of the first nine cycles varies in terms of half-cycle widths and amplitudes. This is shown in fig. 6 for a 15-cycle burst of current having a final value of about 33000 A peak and for a setting of 90% heat. The "power factor" adjusting logic of the controller "massages" the phase of the SCR-control signal, which in turn causes the smoothed output current to vary in amplitude. The amplitudes of the first 9 cycles more or less increase in a ramp-like fashion until stable operation is achieved. Typically, the peak amplitude of the current at the first cycle is about 0.75 of the final amplitude value after 9 cycles. The initial few cycles seem to alternate between lower and higher amplitudes, as shown in fig. 6.

The waveform "massaging" that the controller performs can cause difficulties in determining the beginning and ending of an integral number of complete cycles, which is usually necessary when deriving rms values from digitized waveforms. Additionally, in certain instances, waveform assymetry

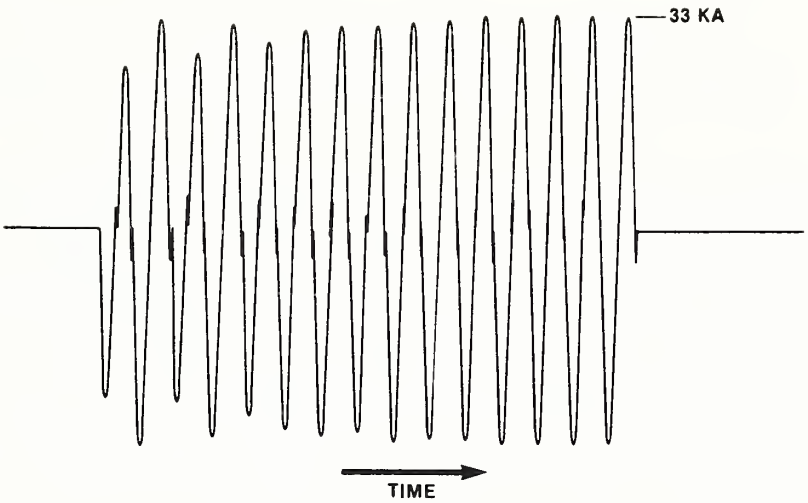

Figure 6. A fifteen-cycle burst of current waveform showing characteristics of the SCR controller "massaging" effects as it adjusts the power factor. Notice that the waveform stabilizes after about the ninth cycle.

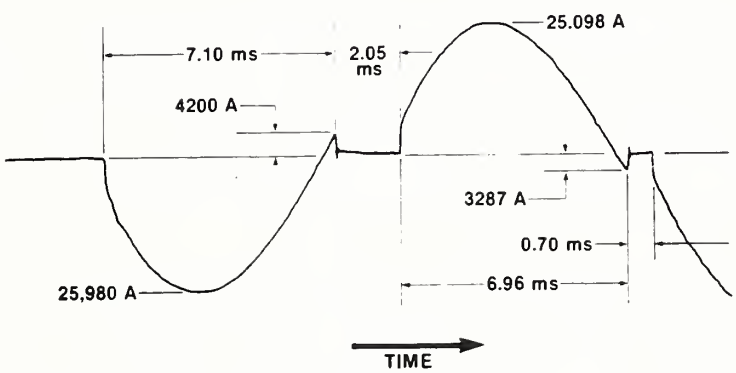

Figure 7. The waveform of the first cycle of a five-cycle burst. Note difference in times and amplitudes as the controller "massages" the waveform for power factor adjustment.

can cause a dc component of current which, in turn, can lead to measurement errors if not properly accounted for and treated. This topic and its effect on the measurement and calibrations process will be the subject of further investigation.

Generally, the measurement and calibration process is easier and less prone to errors if waveform distortion is absent. It is, therefore, desirable to use portions of the waveform after the ninth or tenth cycle for calibration measurements. This is feasible for currents ranging from about 10 kA rms to where a total of about 20 integral cycles can be obtained. When calibrating shunts heat accumulation can be bothersome, however, because of the extra cycles needed for waveform stabilization. For currents greater than about 60 kA rms, operation of fewer than about 20 cycles is necessary to prevent the autotransformer fuses from blowing, and at the maximum current of about 70 kA rms only 3 or 4 cycles can be achieved without the system tripping off.

Interesting waveform characteristics can be observed by closer examination of individual cycles and the switching transients of the SCR-transformer-load combination. Figure 7 shows a time-expanded first cycle of a 5-cycle burst. The test conditions were set for 99% heat and a final current amplitude of about 33 kA peak. The load was as previously described. Of particular interest is the difference of amplitudes of each half cycle which is a direct result of the difference in half-cycle pulse widths. Also note the deviation from a sinusoidal waveform and the "skewed" nature of each half cycle. Figures 8a, 8b, and 8c show details of the switching response at the first, second, and third zero crossings for the first cycle and into the middle of the second cycle. There are 15% current overshoots at turn-offs (figs. 8a and 8b) and a ringing of about 14 to 15 kHz (rise and fall times of approximately 35 μs). Figure 8c shows the turn-on characteristic where the current increases to about 5.5 kA (approximately 20% of the peak amplitude) in about 42 μs.

Of more immediate interest are the characteristics of the current waveform after stabilization occurs, generally after the ninth cycle. A group of data were gathered with the secondary load as previously described using a 10-$\mu\Omega$, 30-kA shunt and an initial stabilized current of about 30 kA peak. The controller was programmed for heat settings ranging from 99% to 0%. Figures 9a through 9m show the results. Figures 10a and 10b show the same results as composite plots without the detailed annotation relating to each test.

As can be seen in comparison with the waveform for the first cycle at 99% heat shown in fig. 7, the switching transient "dead time" for the twelfth cycle, shown in fig. 9a, is considerable less, approximately 0.27 ms (6°), compared with about 2 ms (44.2°) for the first cycle under similar conditions. Little change occurs between heat settings of 99% and 90%, but thereafter, the waveforms become progressively "smaller" as the heat setting becomes less. Finally, at the very lowest settings, no change can be noted between 1% and 0%. (This is rather academic inasmuch as the system is not likely to be used under such conditions, nor would calibration requirements likely be needed under such low heat settings.) Table 2 gives information regarding the output current (rms and peak amplitudes) and half-cycle widths of the current pulses "on-time" and "off-times".

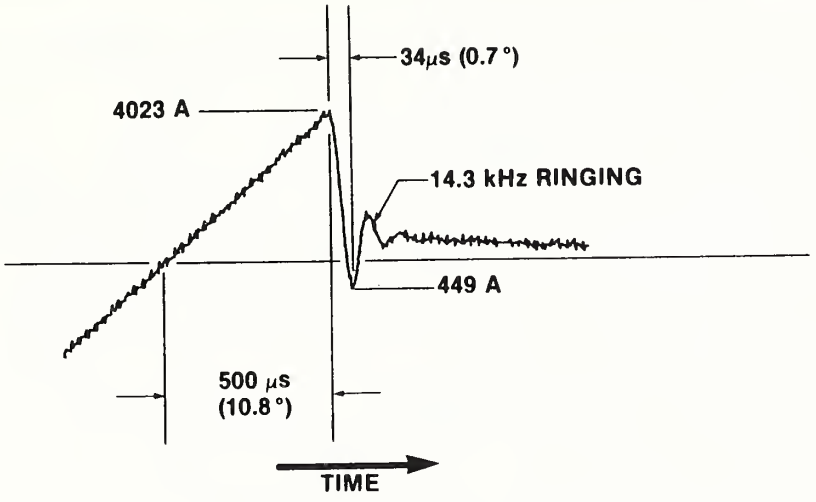

a) First zero-crossing

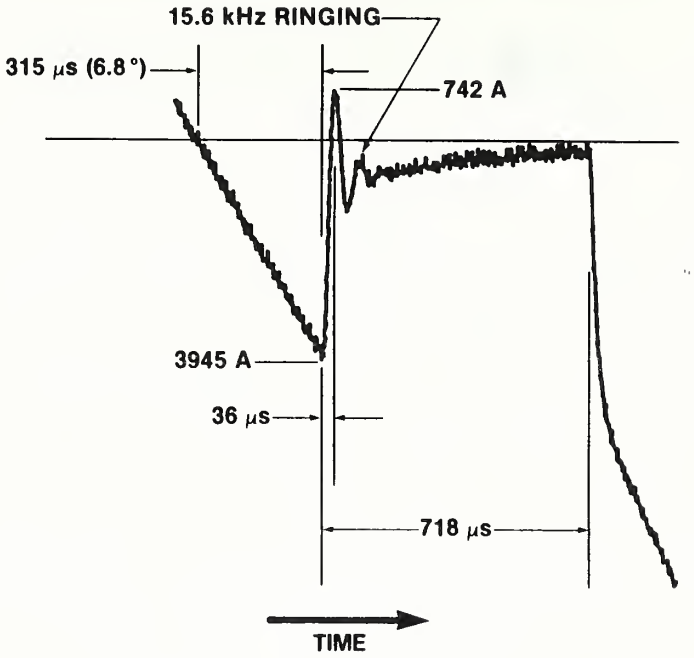

b) Second zero-crossing

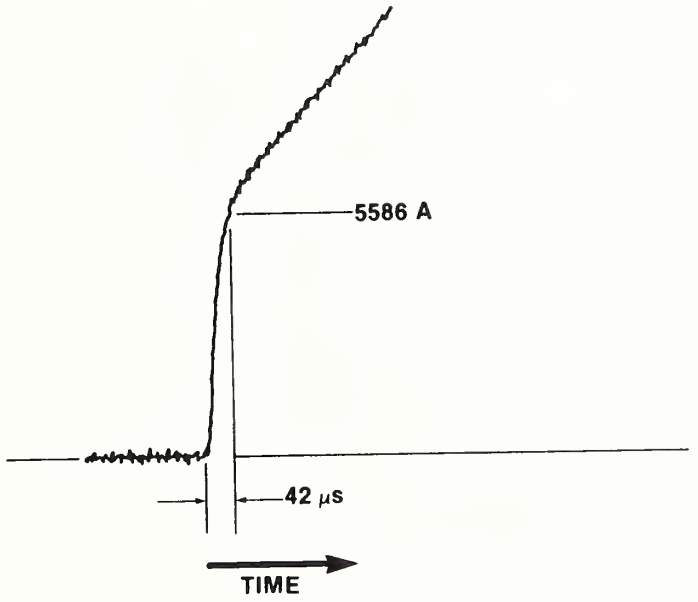

c) Third zero-crossing

Figure 8. Time-expanded waveforms when the SCR's gate on and off;
a) first zero-crossing,
b) second zero-crossing, and
c) third zero-crossing.

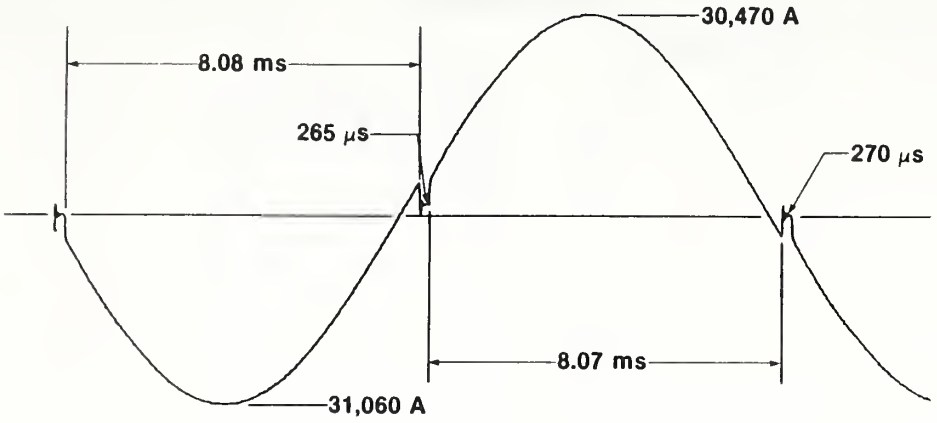

Figure 9a. Waveform of the twelfth cycle for a heat setting of 99%.

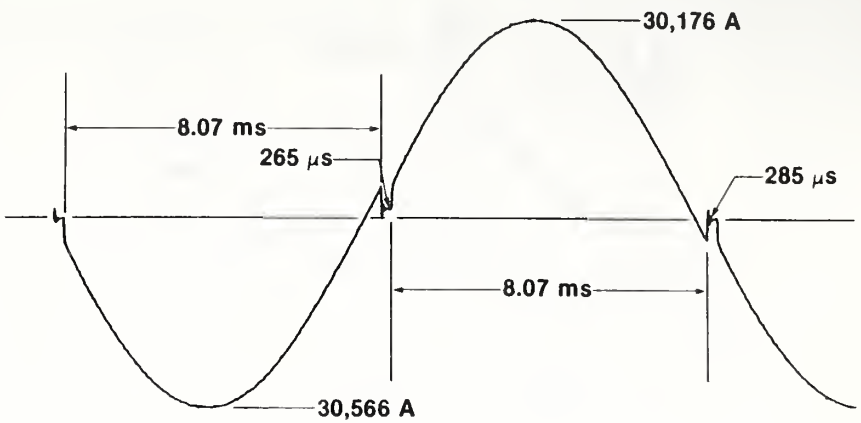

Figure 9b. Waveform of the twelfth cycle for a heat setting of 90%.

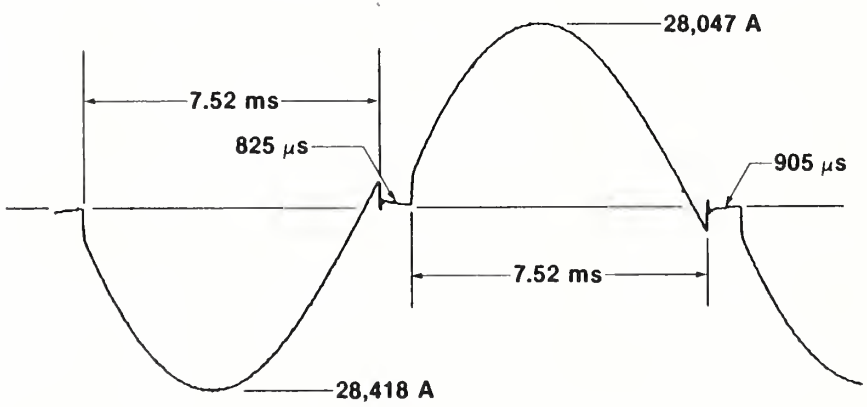

Figure 9c. Waveform of the twelfth cycle for a heat setting of 80%.

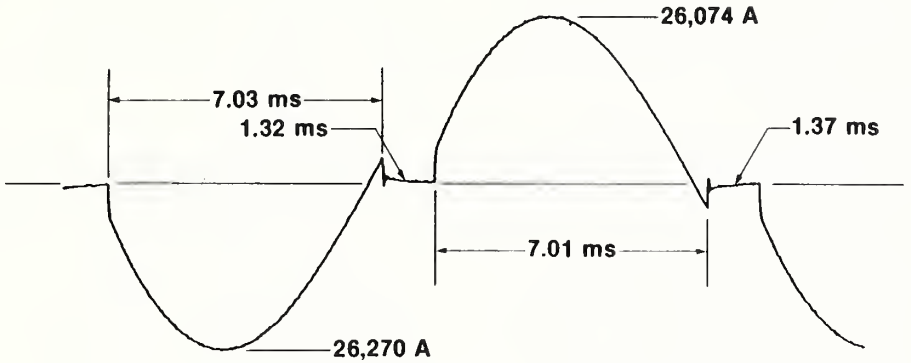

Figure 9d. Waveform of the twelfth cycle for a heat setting of 70%.

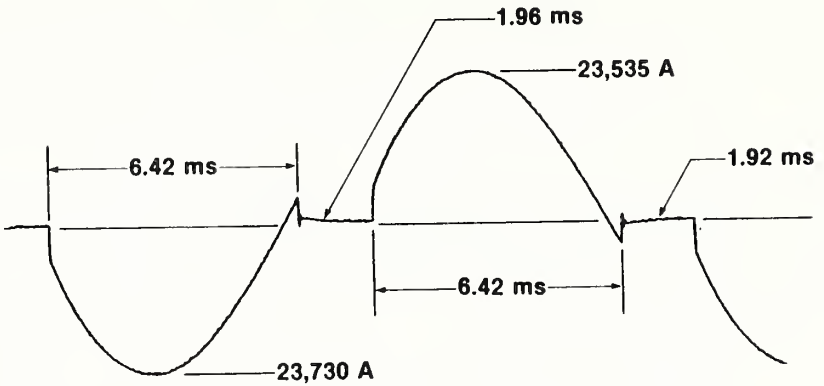

Figure 9e. Waveform of the twelfth cycle for a heat setting of 60%.

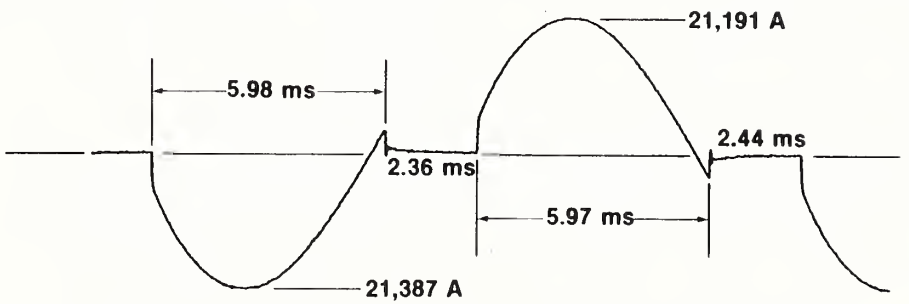

Figure 9f. Waveform of the twelfth cycle for a heat setting of 50%.

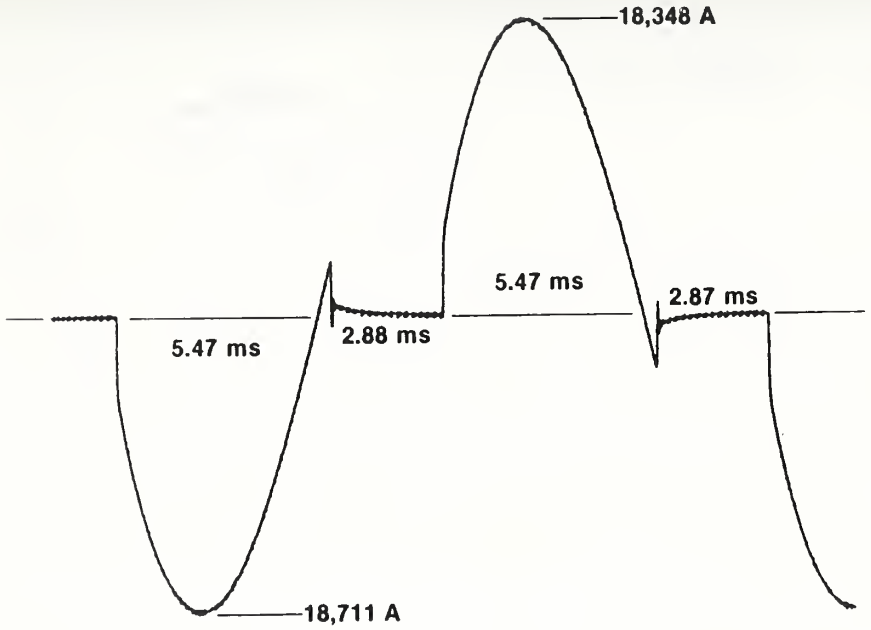

Figure 9g. Waveform of the twelfth cycle for a heat setting of 40%.

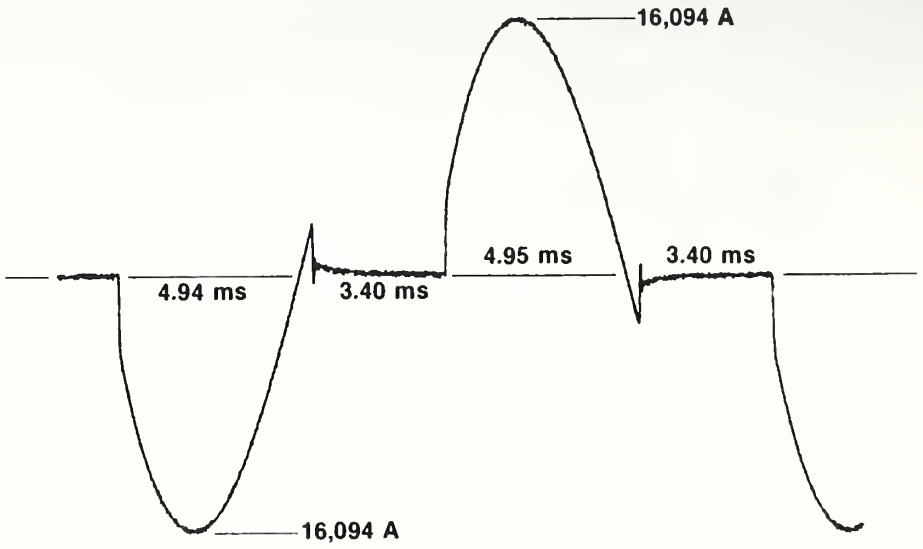

Figure 9h. Waveform of the twelfth cycle for a heat setting of 30%.

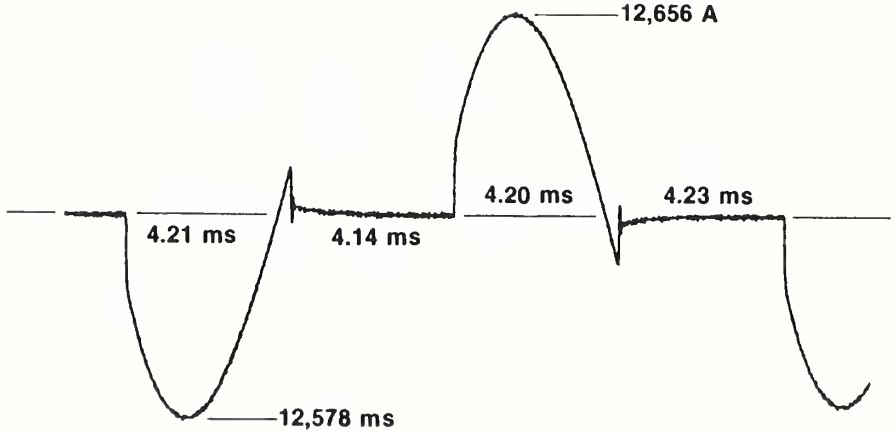

Figure 9i. Waveform of the twelfth cycle for a heat setting of 20%.

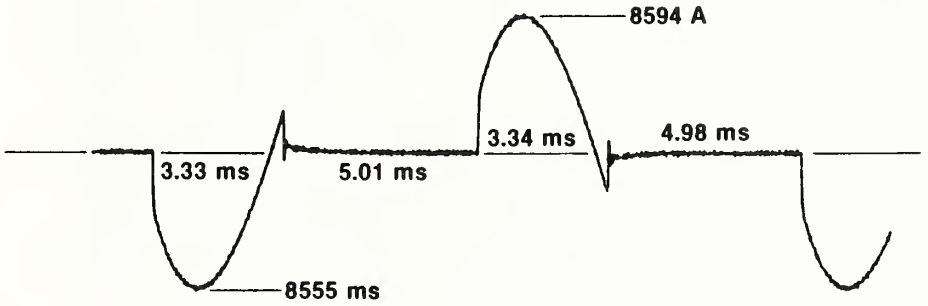

Figure 9j. Waveform of the twelfth cycle for a heat setting of 10%.

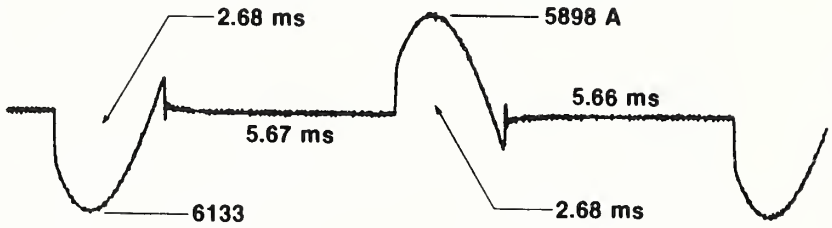

Figure 9k. Waveform of the twelfth cycle for a heat setting of 5%.

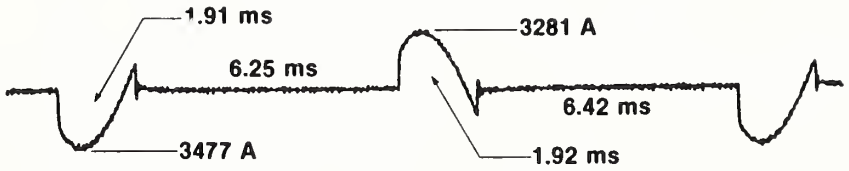

Figure 91. Waveform of the twelfth cycle for a heat setting of 1%.

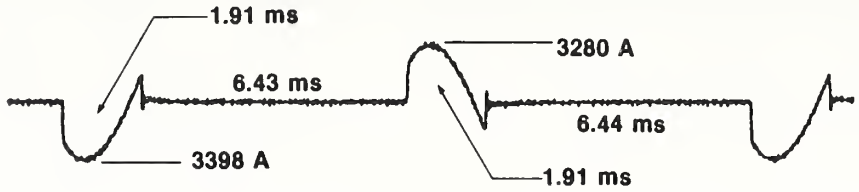

Figure 9m. Waveform of the twelfth cycle for a heat setting of 0%.

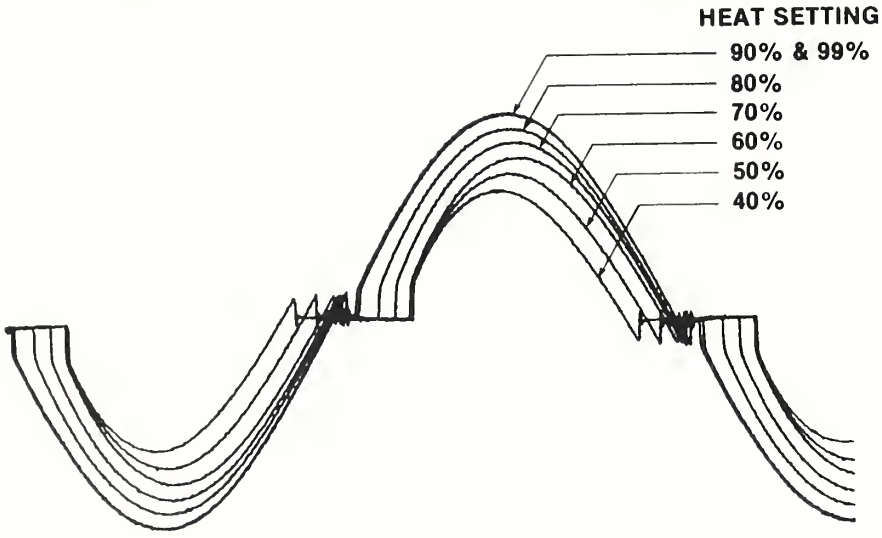

Figure 10a. Waveform composite of twelfth cycle for heat settings from 99% to 40%. (Same as for figures 9a - 9g.)

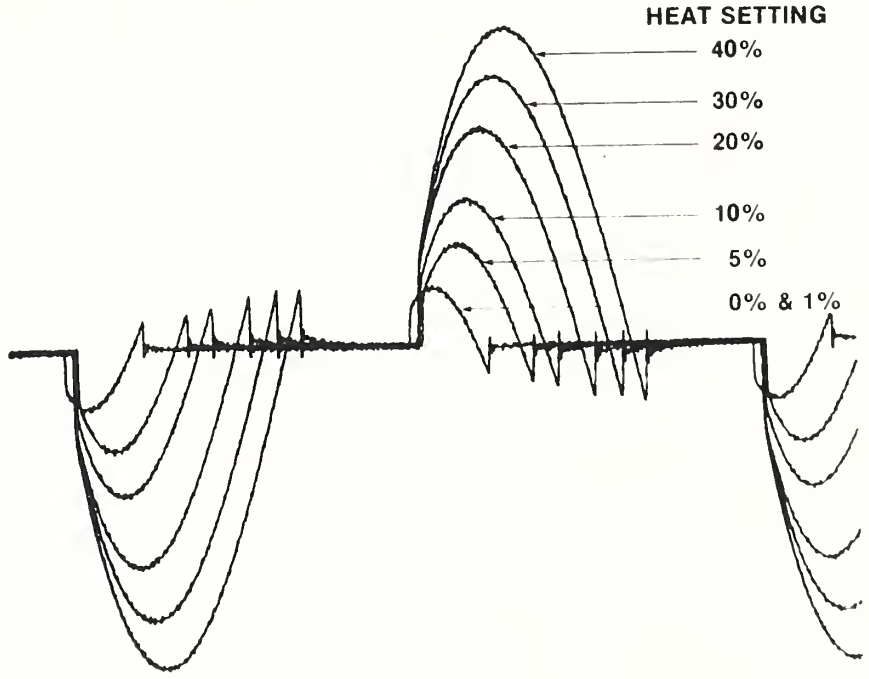

Figure 10b. Waveform composite of twelfth cycle for heat settings from 40% to 0%. (Same as for figures 9g - 9m.)

Table 2. Output current and pulse durations as a function of heat settings. (The valves shown were obtained from a different set of data than that shown in figures 9a-9m.)

Heat Setting (%)	Output Current (kA, rms)	Output Current (kA, peak)	Ratio, I_{rms}@ xx% Heat / I_{rms}@ 99% Heat	Half-Cycle On Time (ms)	Off-Time Between (ms)
99	21.55	31.14	1.000	8.07	0.27
90	21.02	30.12	0.975	8.07	0.27
80	18.76	27.79	0.871	7.52	0.87
70	16.81	25.66	0.780	7.03	1.35
60	14.75	23.29	0.684	6.42	1.96
50	12.99	21.07	0.603	5.98	2.40
40	10.76	18.26	0.499	5.47	2.88
30	8.70	15.52	0.404	4.94	3.40
20	6.28	12.05	0.291	4.21	4.14
10	3.73	7.98	0.173	3.33	5.01
5	2.27	5.43	0.105	2.68	5.57
1	0.99	2.73	0.046	1.91	6.43
0	----	2.73	0.046	1.91	6.43

Figure 11 shows the relationships between the heat settings, the half-cycle pulse widths, and the output current, both peak and rms values. These tests used the same 10-$\mu\Omega$ shunt and bus-bar arrangement previously described. The peak current at 99% heat was approximately 30 kA. Waveforms for each of the measurements are essentially the same as shown in figs. 9a through 9m.

The pulse width plot shown in fig. 11 uses the left-hand ordinate. The output currents use the right-hand ordinates. The actual currents can be read as obtained for these tests. Also shown is the percentage of the "99% current" outputs on the other two ordinates for current. In this way, one can predict the expected current out of the source for other autotransformer settings. A nearly linear rms current is produced as a function of changes in the percent heat settings.

2.3 Fourier Frequency Spectra

Because of the highly distorted nature of the waveforms being generated, measured, and ultimately used in welding systems, it is desirable to obtain information of typical frequency spectra of these waveforms. The spectra have a significant influence on the bandwidth considerations of current sensors being used or calibrated, and on other instrumentation used in the calibration process or welding processes.

Using the short flat copper bus-bar configuration previously described, a 10-$\mu\Omega$ shunt was connected across the output of the current source. Discussions with the shunt's designer and manufacturer indicated that the frequency

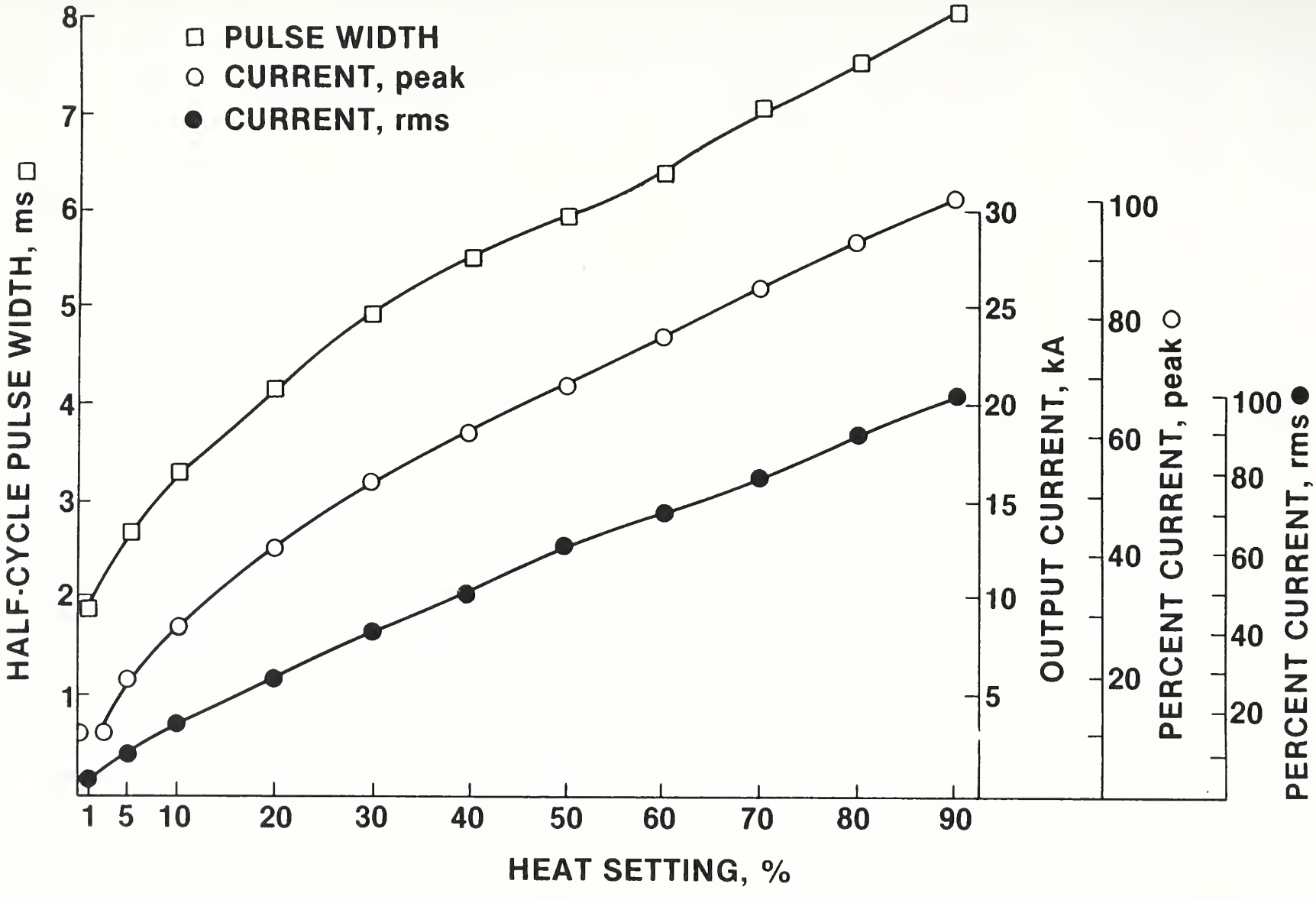

Figure 11. Secondary current half-cycle pulse widths and output current. Right hand ordinates may be used to determine output currents at other autotransformer settings.

response of the shunt was several thousand hertz minimum and would be suitable for making measurements of the approximate spectra of welding currents. Bursts of 20 cycles of current were programmed and the series of tests were conducted over a range of heat settings from 99% and 10% in 10% increments. The typical waveforms for individual cycles can be seen in figs. 9a through 9m. A Fourier analysis was used to derive the amplitude of the harmonic series for frequencies up to the fifteenth harmonic of 60 Hz, or 900 Hz. Table 3 gives the results of these measurements. The values given are expressed as a percentage of the 60 Hz component. As expected, the amount of harmonic content increases as the heat settings decrease. In all instances, the major energy is contained in the fundamental and the low-order harmonics, namely, the third, fifth, and seventh.

Figure 12 shows a plot of the harmonic content as a function of the heat setting. Figure 13 shows a typical spectrum for the heat setting of 20%. Note that the third harmonic is by far the greatest, with the other components being very much smaller. (The fundamental has been removed from these plots to permit expansion of the harmonic data.) Because only an estimate of spectra was needed, no antialiasing filters were used. As a result, with a Nyquist frequency of only 1 kHz, aliasing is apparent in the results as shown in fig. 13. Note the frequency components spaced every 40 Hz which may contaminate the data, especially the higher order harmonics where their amplitudes are relatively small.

For the resistive and inductive load on the current source, it is apparent that frequency components greater than 1 kHz are of little concern and that the most significant energy is contained in the low order harmonics. It is also necessary to remember that the amount of distortion that is contained in the SCR-chopped waveforms is a direct function of the nature of the current transformer and the load. For these measurements and data, the load impedance is very small, and very little smoothing of the current waveform occurs. With other larger loads typical of calibration setups and certainly typical of welders, significantly more smoothing will occur and the harmonic content will be reduced accordingly. In welding applications, it is common practice to measure the rms value of current. Also, in the calibration procedure discussed later in this report, the ratio of rms quantities are used. In both cases, utilizing the rms properties is a "forgiving" process, and decreases the importance and contributions of the low amplitude, higher order harmonics.

2.4 Magnetic Field Strength Near Output Transformer

Measurements were made to determine the approximate strengths and directions of the magnetic fields in the vicinity where current sensors, such as shunts and Rogowski coils, might be placed for measurements. Also of concern was the possibility of these fields interfering with sensitive instrumentation near the transformer, such as oscilloscopes, digitizers, and equipment having magnetic tape or disks. A further concern was exposure of personnel working near the transformer.

The magnetic field originates from two main sources, first the field created as a result of the current flowing through the secondary bus, and secondly, other fields such as from transformer flux leakage. The field is then the vector sum of all fields at any location. A calibrated magnetic

Table 3. Harmonic content in the output current as a function of heat settings. Content given as a percentage of the 60-Hz fundamental.

Harmonic of 60 Hz	Harmonic Frequency (Hz)	Harmonic Content Referenced to 60-Hz Fundamental								
		Heat Setting								
		10%	20%	30%	40%	50%	60%	70%	80%	90%
3rd	180	81.3	64.1	51.3	39.4	30.5	24.2	16.5	9.8	2.8
5th	300	36.1	10.8	3.9	8.9	10.3	9.9	8.0	5.3	1.3
7th	420	4.7	12.8	10.1	3.2	2.4	4.7	5.3	3.6	1.1
9th	540	12.3	4.9	4.1	5.0	2.8	0.7	2.4	2.9	0.8
11th	660	8.2	6.2	3.5	2.7	3.5	2.1	1.0	2.2	0.6
13th	780	4.3	3.3	3.6	1.3	1.7	2.4	0.7	1.3	0.7
15th	900	7.4	3.9	1.0	2.4	0.9	1.8	1.3	0.9	0.6

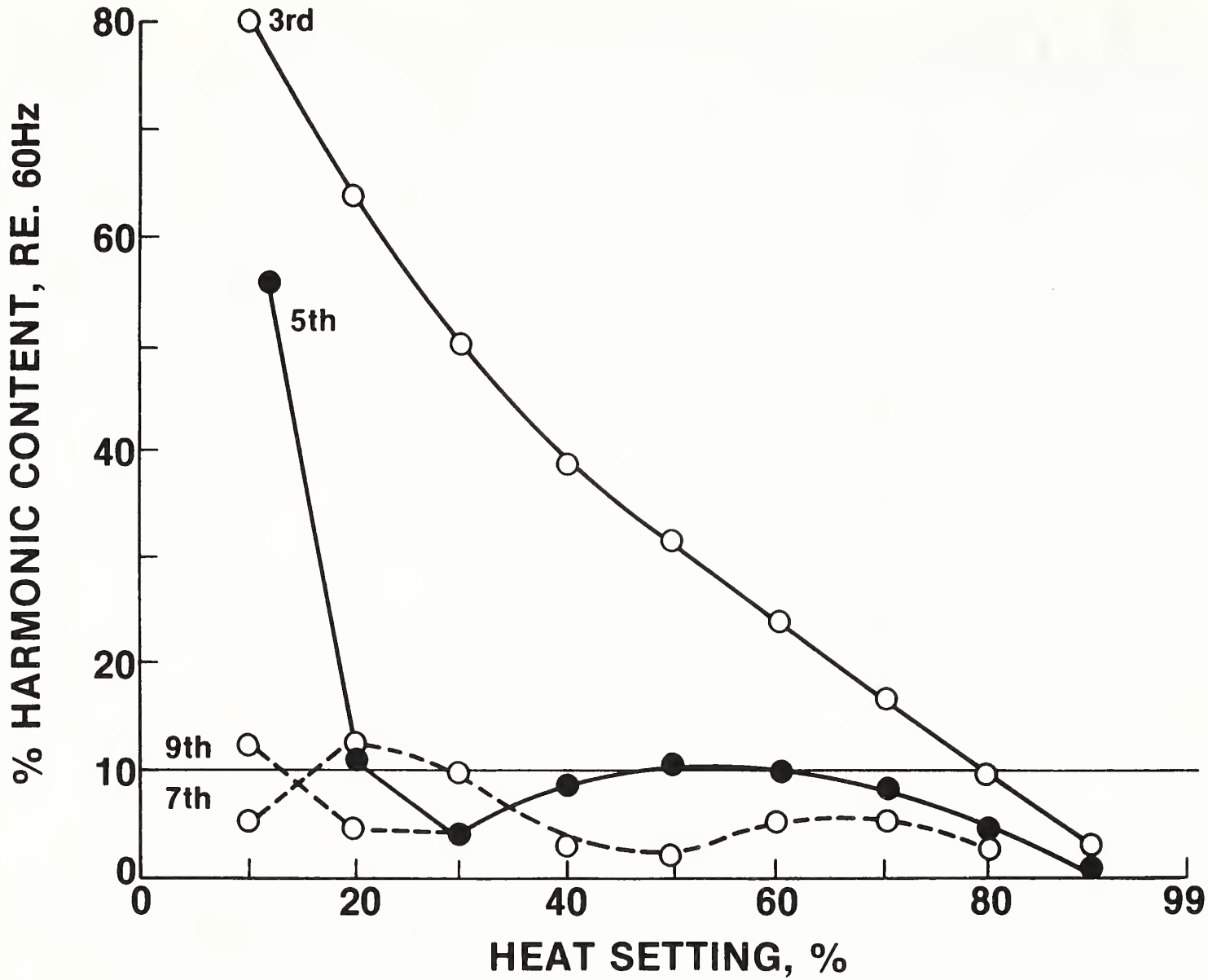

Figure 12. Harmonic content in output current as a percentage of the 60-Hz fundamental.

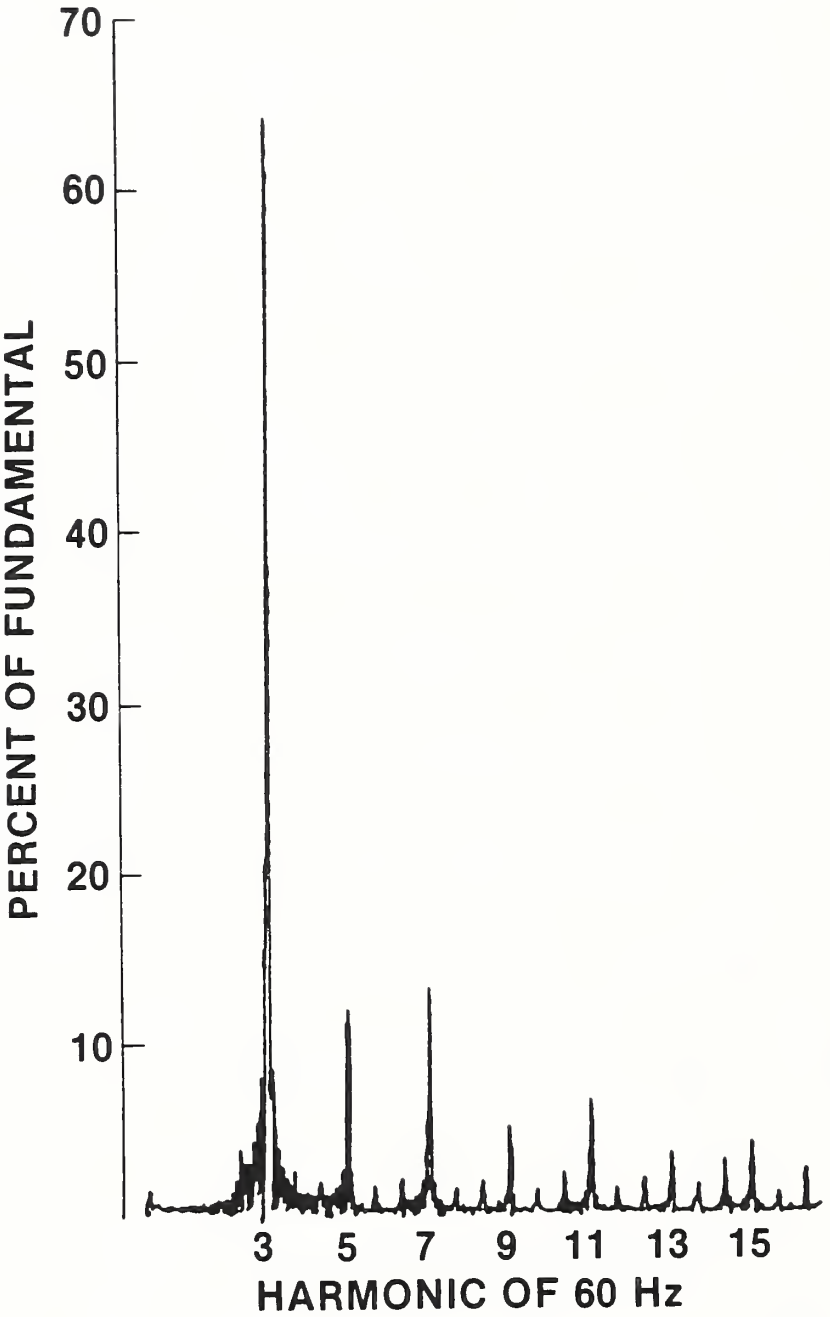

Figure 13. Harmonic spectra in the output current for a heat setting of 20%.

field meter was used which could sense both the magnitude and direction of the field.

Table 4 gives the results of the measurements. The measurement location of the magnetic field sensor is indicated by a x-y-z coordinate system defined in fig. 14. Distances from the central axis of the output transformer were used to define the measurement location (expressed in centimeters). The field was measured in units of microtesla rms, and the secondary current producing the field was measured in units of kiloamperes rms. (The current was not measured for each individual magnetic field measurement; in those instances a nominal value was used, denoted by "nom" after the value of current in the table. The nominal value was determined from measurements made at nearly the same time. The nomenclature, "mea" after the value of current indicates that the current was measured.) The final three columns of table 4 show normalized values of the field in units of tesla per ampere. This allows a computation of the field to be expected from any secondary current with the previously described bus arrangement.

The maximum field can be determined by finding the vector sum of b_x, b_y, and b_z (i.e., the square root of the sum of the squares), and the results are denoted as b_{max} in the last column of table 4. For these sets of measurements, the maximum field was at location 2 and had a value of about 1700 μT rms with a secondary current of about 16 kA rms. This location was very near the "throat" of the current loop formed by the flat copper bus plates to connect to a shunt. At full output currents of 100 kA peak, the maximum field strength is estimated to be 7500 μT peak (7.5 gauss peak). At more distant locations, the field was very much smaller.

These results apply to this transformer with this particular geometric arrangement for the secondary current. Other secondary bus-bar arrangements will produce different fields, but the measurement results shown can be used to develop a sense of the problem of stray magnetic fields.

3. HIGH-CURRENT SHUNT AND ROGOWSKI COIL CALIBRATION TECHNIQUE

Welding systems typically employ a high-current shunt or a Rogowski coil to sense the weld current. In either instance, it is necessary to calibrate these current sensors for reasons of quality control of the welding process. Either a shunt or a Rogowski coil can be calibrated in place by using a calibrated transfer standard. A calibration method which uses the ratio of rms voltages is described in this section. Estimates of measurement uncertainties are also given.

3.1 Calibration Procedure and Philosophy

Figure 15 shows a typical calibration arrangement for determining the calibration constants for either a resistive shunt or for a Rogowski coil with an integrating amplifier. The current source is used to generate a test current, I_t, which is sensed by the three sensors in the circuit. The shunt develops a voltage drop, V_s, which is at the output of a RC frequency compensating network. The Rogowski coil and amplifier combination generate an

Table 4. Results of magnetic field strength measurements for 250-kVA transformer measured and the locations indicated. Also see Fig. 14.

Test Location Number	Position from Transformer Central Axis cm			Measured Magnetic Field Strength and Sec. Current Tesla x 10^{-6}, rms kA, rm			Normalized Magnetic Field Strength (Tesla/A) x 10^{-9}			
	x	y	z	B_x	B_y	B_z	b_x	b_y	b_z	b_{max}
1	24	20	0	130 15.96 nom	210 15.96 nom	580 15.96 mea	8.14	132	36.34	39.5
2	24	2	0	1,740 15.96 nom	140 15.96 nom	340 15.96 nom	109	8.78	21.3	111.4
3	24	-34	0	310 15.87 nom	110 15.87 nom	350 15.87 mea	19.53	6.93	22.05	30.7
4	130	-34	0	26 15.76 mea	5 15.76 mea	4 15.58 mea	1.65	0.05	0.36	0.37
5	130	2	0	31 15.77 mea	8 15.76 mea	5 15.75 mea	1.99	0.51	3.2	20.5
6	130	20	0	24 15.76 mea	4 15.75 mea	13 15.76 mea	1.52	0.25	0.82	1.75
7	24	2	100	29 15.60 mea	21 15.54 mea	12 15.54 nom	0.77	1.35	1.86	2.05

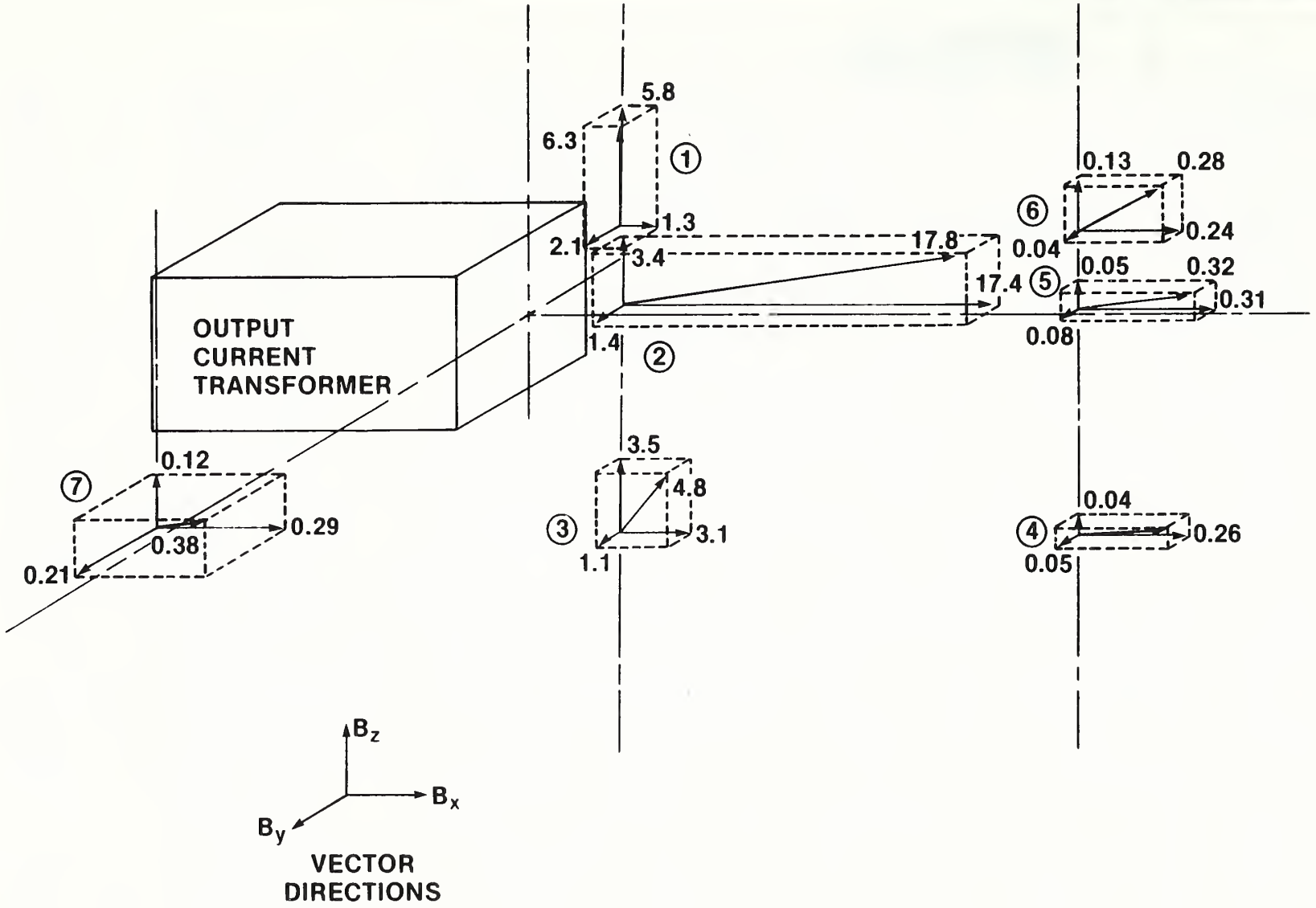

Figure 14. Magnetic field strengths at various locations near the output transformer. Refer to table 4 for distances which are keyed to the numerals in circles. Values given here are in units of gauss rms for nominal secondary currents of 16 kA rms. (1 gauss = 100 μT).

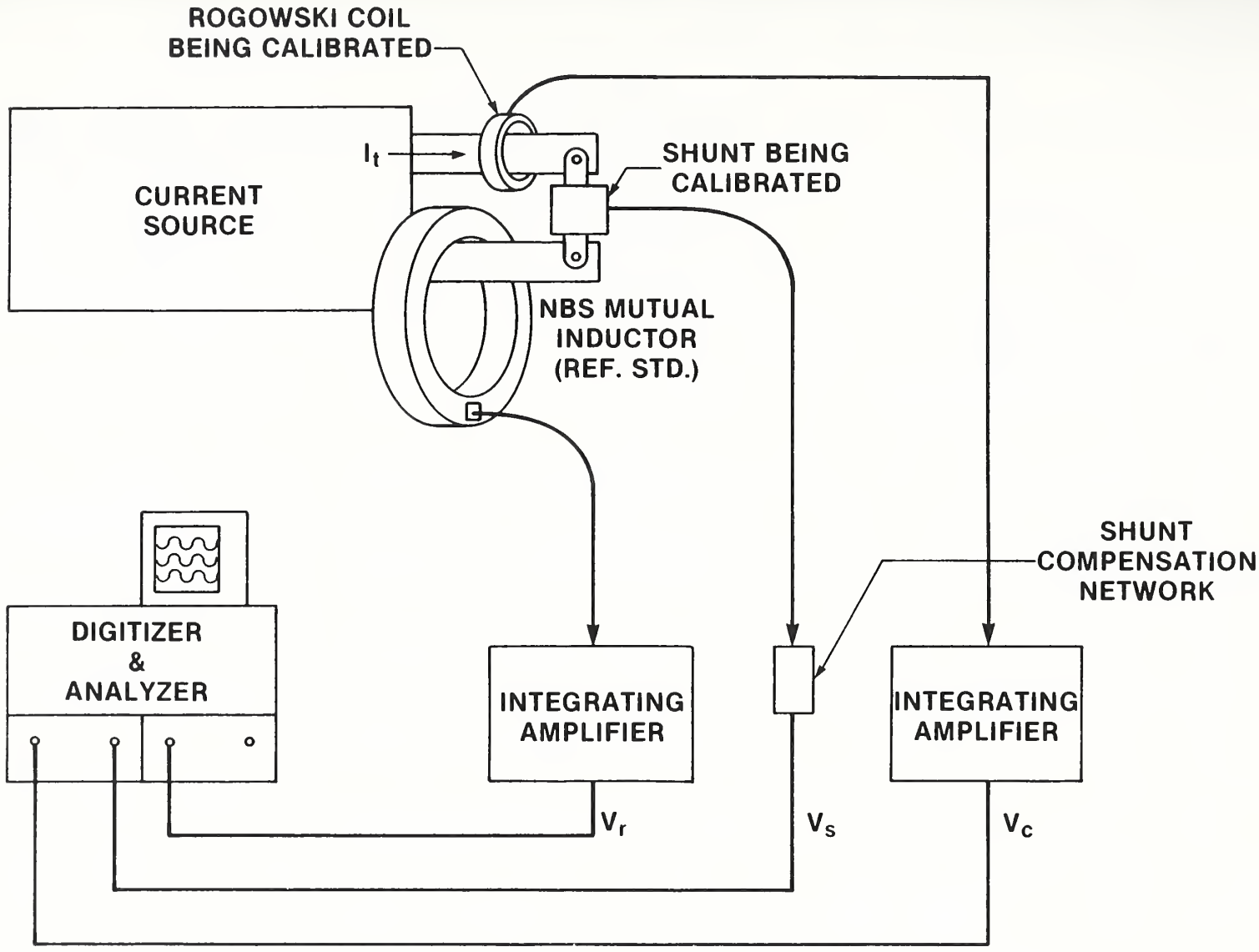

Figure 15. Block diagram showing typical calibration arrangement for a shunt and a Rogowski coil, each to be calibrated using the NBS mutual inductor as a reference. (Floppy disk unit used with the digitizer not shown.)

output voltage V_c. A reference-standard current-sensing mutual inductor[1], NBSMI, and its associated integrating amplifier, NBSIA, develop a voltage V_r. Using combinations of these voltages, and knowing the transimpedance of the standard (NBSMI and NBSIA combination), it is possible to calibrate either the shunt or Rogowski coil/amplifier being tested.

The following equations describe the electrical relationships used in the calibration process:

$$V_s = I_t Z_s, \tag{1}$$

$$V_c = I_t Z_c, \quad \text{and} \tag{2}$$

$$V_r = I_t Z_r, \tag{3}$$

where V_s is the output voltage of the shunt,

V_c is the output voltage of the Rogowski coil/amplifier combination,

V_r is the output voltage of the reference standard, NBSMI/NBSIA combination,

I_t is the test current applied to all sensors,

Z_s is the effective shunt impedance,

Z_c is the transimpedance of the Rogowski coil/amplifier combination, and

Z_r is the transimpedance of the NBSMI/NBSIA combination.

The transimpedance of a Rogowski coil/amplifier combination, the shunt, or the mutual inductor/amplifier combination is defined as the ratio of the output voltage to its input current, and can be thought of as a transfer function. Using the above relationships, the shunt's impedance or the coil/amplifier transimpedance can be determined as

$$Z_s = [V_s/V_r]Z_r \quad , \text{and} \tag{4}$$

$$Z_c = [V_c/V_r]Z_r \quad . \tag{5}$$

The voltages can be digitized and the rms values determined by the use of a digitizer and microprocessor-based analyzer. The original waveforms can be stored on a medium such as a floppy disk for future use. The digitizer used for the measurements described herein had 10-bit digital resolution. The sampling rate was generally selected (0.2 ms/sample) so that a burst of 9 cycles of the test current was digitized having 750 samples. The 10-bit

---

[1]The reference standard, NBSMI, can be analyzed either as a mutual inductor or a Rogowski coil. In this report, it is used as a mutual inductor having an output voltage of M di/dt, where M is the mutual inductance (nominally 1 μH) and di/dt is the first time derivative of current.

digital resolution is barely adequate for the measurement results, and the use of 12- or 14-bit digitizers would be preferred.

It is important in the data analysis to determine the rms voltages of the two waveforms simultaneously. Because there can be cycle-to-cycle amplitude variations in the input voltage to the current source, analyzing each waveform for exactly the same nine cycles is essential to minimize measurement errors. The nine-cycle period is generally set by selecting the beginning or ending point, and then indexing an appropriate 150 ms, rather than depending on such criteria as zero crossings, etc. to set both ends of the nine-cycle period. It was also determined that better results were obtained when dc levels were removed from the measurements. These were removed using the computational capabilities of the analyzer.

3.2 Initial Shunt Calibration Results

Initial calibration measurements were performed on a 30 000-A, 10-$\mu\Omega$ shunt commonly used for measuring welding currents. The shunt was connected between rigid flat bus-bar plates which were mounted directly onto the output pads of the main transformer. The system configuration shown in fig. 15 was used where the output voltages of the shunt, V_s, and of the NBSMI/NBSIA reference standard, V_r, were connected to the inputs of the digitizer. These tests were performed at currents of nominally 30 000 A peak, at a heat setting of 99% for 24 cycles, and at one minute intervals.

The first sets of data suggested that the effective shunt resistance was changing as a function of successive tests and shunt heating was suspected to be the cause. Data were collected along with measurements of the shunt temperature. Thermocouples were mounted at various locations on the shunt. Direct measurement of the temperature of the manganin shunt material is difficult because it is encapsulated with an electrical insulating material. It was arbitrarily decided that data would be referenced to the temperature at a location nearest the manganin material on the top of and midway between the ends of the shunt.

Figure 16 shows the results of three sets of measurements where the shunt resistance is plotted versus the shunt temperature as described above. It was surprising that any temperature coefficient could be measured inasmuch as the temperature coefficient of resistance for manganin is very low. Typical values of temperature coefficient of resistance for annealed manganin wire are perhaps 2 to 10 ppm/°C, while for flat rolled strip manganin, which has also been annealed, the coefficients may be between 5 to 30 ppm/°C. Other forms of manganin may be used to fabricate high-current shunts and the temperature coefficients for such use of the material are not known, although they should be relatively low. For the range of temperatures observed in these tests, changes in shunt resistance as large as 0.1% were noted. Changes greater than perhaps 0.02% would be considered large. Sufficient measurements were made to verify that the resistance was changing as a function of temperature. It is speculated that the temperature coefficient is very large, or that the cause is temperature induced strain.[1]

The upper curve of fig. 16 (shown by "open circles") was obtained as described above with the shunt rigidly mounted between the heavy copper bus-bar plates. In this configuration, the shunt was physically constrained and

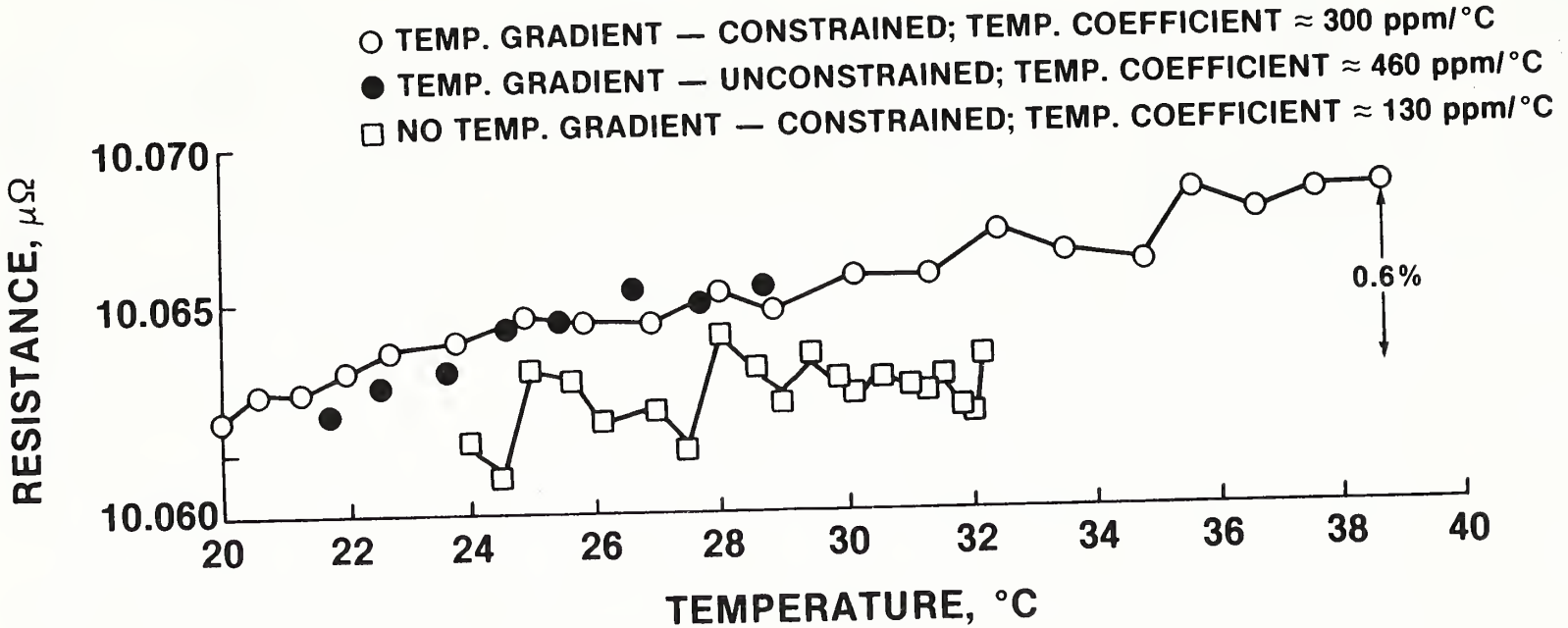

Figure 16. Calibration results for a 30-kA, 10-μΩ shunt for various test conditions. Refer to text for explanation of test conditions.

thermal stresses could build up. The temperature coefficient for this test was approximately 300 ppm/°C. However, when one end of the shunt was removed from the rigid mounting and replaced with a flexible link, the temperature effect did not decrease as anticipated, but indeed increased somewhat to about 460 ppm/°C. (This is shown in fig. 16 by "solid" circles.) It was therefore concluded that the bus-bar arrangement was not constraining the shunt and causing the problem.

It was noted during the testing that one of the shunt mounting lugs was being heated much more than the other, perhaps by as much as 16°C. Considering that each was mounted to massive copper plates, this led to an investigation of the mating surfaces of the shunt lugs. It was apparent that during the manufacture of this shunt, the lugs had been solder dipped and an uneven surface resulted. There were several locations on the surface of the lug where the solder had formed "globs" of perhaps 3 to 5 mm in diameter. Additionally, the shunt had at some time been mounted without care and the surface surrounding the mounting hole was severely rough thus creating uneven mounting conditions.

The shunt surfaces were dressed flat and smooth, and the tests were repeated. The differential temperature of uneven lug heating reduced drastically to a temperature difference measured to be less than 2°C. The lower curve of fig. 16 (shown as "squares") gives this result. The temperature coefficient was measured to be approximately 130 ppm/°C. This value, although more than ten times that expected, was certainly less than that when a temperature differential or gradient existed across the shunt as in the previous two tests. It is therefore concluded that this shunt is likely to be accumulating internal stress sufficient to strain the manganin material in such a manner to change the effective resistance.

Two additional shunts of the same design were tested under the same conditions and similar results were obtained. Figure 17 shows the results of one of them. The measurement results are in terms of the rms voltage ratio, V_s/V_r, and plotted as a function of the shunt temperature. A least squares regression analysis was done to determine the best fit of the data to a straight line. The regression "end-points" are shown for temperatures of 24°C and 36°C. The slope of these curves are approximately 140 ppm/°C which is about the same as the other shunts tested.

The lower of the two curves shown in fig. 17 was derived without the dc-voltage component being removed from the data analysis, whereas in the upper of the two curves the dc-voltage component was removed. (The dc-components in both of the voltage waveforms can come from offsets in electronic instrumentation used to make the measurements, especially when using dc-coupled integrating amplifiers, and from waveform asymmetry.) The removal of the dc-voltage components from both waveforms resulted in a positive shift of the results of about 0.1%. This and other tests suggest that more accurate results can be obtained when the dc-voltage components are removed. This will be the subject of further investigation.

The temperature build-up observed during these tests are probably more severe than those expected in most welding applications. In practice, fairly long periods exist between welds, perhaps 5 to 15 minutes or more. In such cases, the shunt can cool between use, and temperature increases of only a few

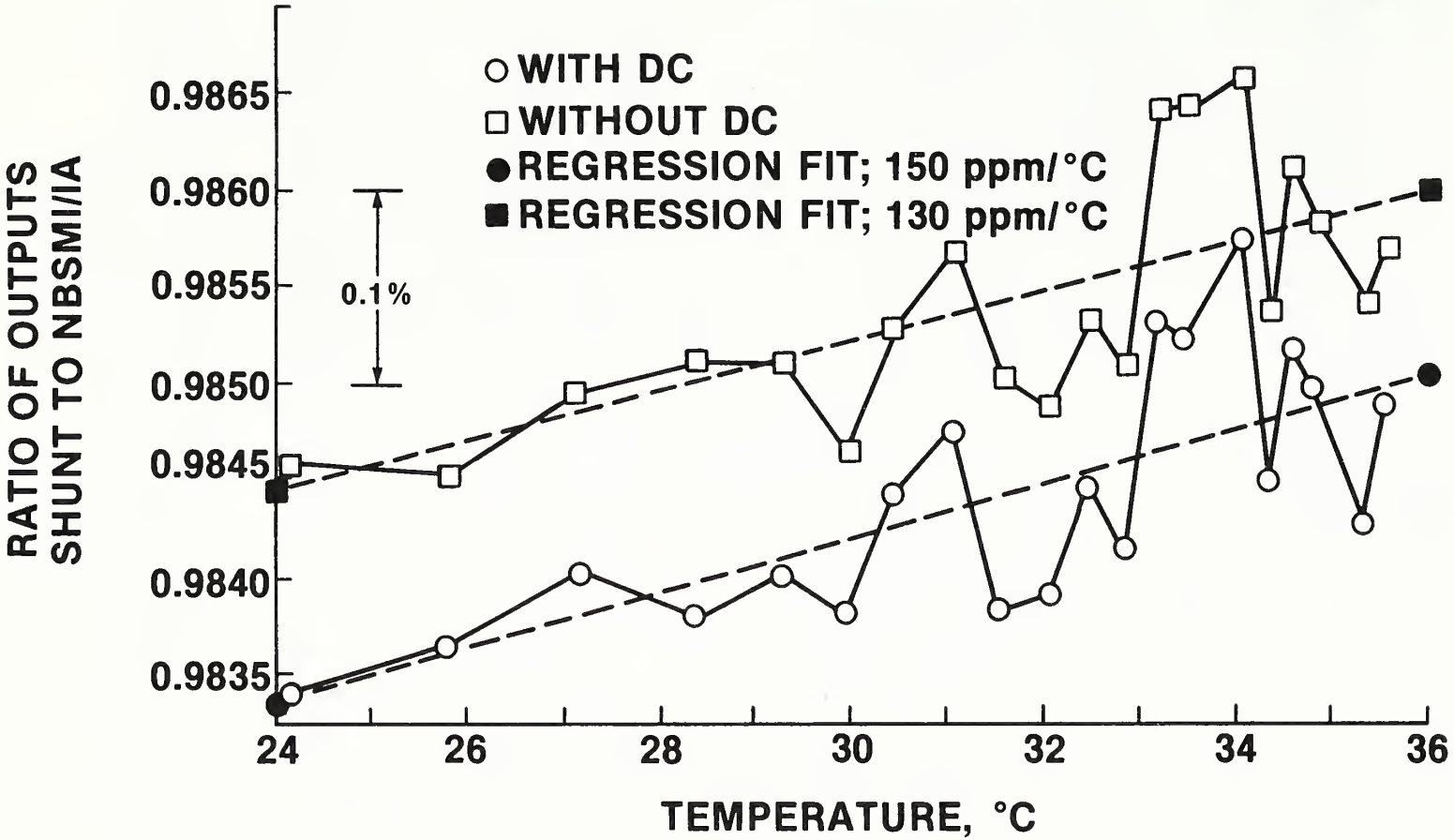

Figure 17. Calibration results for a 30-kA, 10-μΩ shunt as a function of shunt temperature. Lower plot is an analysis with data containing a small dc-component, while the upper plot is the same analysis with the dc-component removed.

degrees would be expected. It is anticipated that for currents greater than 20 000 or 30 000 amperes, the calibration process will be complicated by the effects of shunt heating. Further tests are planned to explore the nature of the effects observed.

3.3 Rogowski Coil Calibration Results

Three Rogowski current sensing coils were calibrated using the NBSMI/NBSIA combination as a reference standard. The system configuration shown in fig. 15 was used where the output voltages of the Rogowski coil being tested along with its integrating amplifier, V_c, and of the NBSMI/NBSIA reference standard, V_r, were connected to the inputs of the digitizer. These tests were performed at currents of nominally 30 000 A peak, at a heat setting of 99% for 24 cycles. The relationship given by eq. (5) was used to derive the transimpedance of the coil/amplifier combination as previously discussed.

Two of the coils were of a split ring design, that is, they are hinged such that the coil will "swing" open to allow mounting it around the current carrying conductor. One had a window diameter of 12.7 cm and the other, a 2.5-cm window. The remaining sensor was a fixed coil having 6.4-cm diameter window. The 12.7-cm and the 6.4-cm coils were centered on 6.4-cm copper bus-bars for testing. The bus-bar configuration for these tests consisted of 6.4-cm round, solid copper busses which formed a square loop approximately 30 cm wide and 76 cm high. The busses were mounted directly onto the output transformer pads. The coil was positioned such that its axis was centered about the conductor. The 2.5-cm coil was mounted on a 2.5-cm flexible cable. In testing each coil, data were obtained for at least four rotational positions of the coil about the current conductor. Multiple readings were taken at each position to assess the measurement process repeatability.

3.3.1 Test Results for the 12.7-cm Split Coil

Table 5 gives the results of the test performed on the split Rogowski coil having the 12.7-cm window. Tests A(1) and A(2) were repeated measurements, however, the coil was inadvertently bumped during the fifth measurement of test A(1) causing the coil's position to change. This led to an unusually large standard deviation for that data set. Normally, the standard deviation for a set of five or more measurements will be less than ±0.05%. The coil was rotated in nominal increments of 90° between data sets. This was not possible for data set D at an angle of 270° because of mechanical interference between the return bus-bar and the hinged end of the coil. Instead, two sets of data were obtained at rotations of about 270° ±15°, as shown in table 5 as tests D and D'. Tests A' and A were repeats of tests A(1) and A(2). Additionally, measurements were made at other locations on the bus; variations of several percent are easily obtained by doing this.

A pooled mean was calculated by combining all the data for each position, then calculating the mean, as shown at the bottom of table 5. The mean value for the coil/amplifier transimpedance was 3.74×10^{-6} ohm. The change in transimpedance as a function of rotational position was measured to be about 17%, a very large value. For high quality, precision coils, the

transimpedance would not be expected to change more than a few tenths of one percent.

The amplitude linearity was measured over a range of currents from about 6 to 24 kA rms. Table 6 gives the results. The transimpedance was measured to be about 4.145×10^{-6} ohm with very small and insignificant changes from about 11 to 24 kA. The measurements made at about 6 kA indicated a slight increase of about 0.3%. This is thought to be the result of noise in the signals being measured and of differences in the digitizing oscilloscope caused by range changes. It is concluded that there were no significant changes in coil/amplifier transimpedance over the range of currents tested.

3.3.2 Test Results for the 6.4-cm Fixed Coil

The 6.4-cm Rogowski coil was tested similarly to the 12.7-cm coil. Centering on the bus-bar was much easier inasmuch as the window diameter and the bus-bar diameters were nominally equal. Table 7 gives the results of two separate tests where the coil was mounted on different portions of the bus-bar. This was done to determine differences in the coil's response for different nonlinear fields. Differences between the mean transimpedances for the test at the first location and the second were about 0.3%, and thus considered insignificantly small for these tests. The worst case difference in measured transimpedance for rotational positions was about 2% for the first set of tests, and when tested at the second bus-bar location, the differences were less than 0.4%. The grand mean transimpedance for the 6.4-cm coil, derived as shown in table 7, was 3.78×10^{-6} ohm.

3.3.3 Test Results for the 2.5-cm Split Coil

Tests were performed on a Rogowski coil having a 2.5-cm diameter window. This split coil was mounted on a 2.5 cm flexible cable. It was necessary to secure the flexible cable to keep it from flailing during the current impulses. Table 8 gives the measurement results. The coil was rotationally positioned about the cable, similar to the tests for the 12.7-cm and 6.4-cm coils discussed above. The 2.5-cm coil has a sensitivity about 10 times greater than that of the other two coils. Change in the measured transimpedance as a function of rotational position was about 3%, less than the 12.7-cm coil, but greater than the 6.4-cm coil. The individual results were combined into a pooled mean as shown in table 8. A second test was performed at a different location along the flexible cable at an arbitrary rotational position. The result of this is shown in table 8 as test E. It differed from the previous test result mean by about 1.8%, within the range of expected changes that resulted from the rotational test. The measured coil/amplifier transimpedance was 36.1×10^{-6} ohm.

Table 5. Measurement results for a 12.7-cm diameter split Rogowski coil.

Test Position Designation	Coil Position Rotation (degrees)	Coil/Amplifier Transimpedance (x 10^{-6} ohm)	No. of Meas.	Std. Dev. ±(%)	Diff. from Mean (%)
A(1)	0	4.081	5	0.58	+9.2
A(2)	0	4.050	7	0.03	+8.3
B	90	3.523	7	0.04	-5.8
C	180	3.549	7	0.05	-5.1
D	270 (-15)	3.787	7	0.03	+1.3
D'	270 (-15)	3.764	7	0.06	+0.7
A'	360	4.144	7	0.05	+10.9
A(3)	0	4.146	7	0.04	+10.9

Pooled Mean:

$[A(1) + A(2) + A' + A(3)]/4 = 4.105 \times 10^{-6}$ ohm

$B = 3.523$

$C = 3.549$

$[D + D']/2 = 3.776$

14.953 Sum

Pooled Mean = $[14.953/4] = 3.74 \times 10^{-6}$ ohm

Table 6. Amplitude linearity measurement results for a 12.7-cm diameter split Rogowski coil.

Test Current (kA, rms)	Coil/Amplifier Transimpedance (x 10^{-6} ohm)	No. of Meas.	Std. Dev. ±(%)
6.42	4.160	7	0.08
11.20	4.145	7	0.08
19.76	4.145	7	0.05
19.76	4.146	7	0.04
24.10	4.144	11	0.04

Table 7. Measurement results for a 6.4-cm diameter fixed Rogowski coil.

Test Position Designation	Coil Position Rotation (degrees)	Coil/Amplifier Transimpedance (x 10^{-6} ohm)	No. of Meas.	Std. Dev. ±(%)	Diff. from Mean (%)
A(1)	0	3.764	7	0.03	-0.3
A(2)	0	3.770	7	0.03	-0.1
A(3)	0	3.779	7	0.02	+0.1
A(4)	0	3.712	7	0.03	-1.7
B	90	3.780	7	0.02	+0.1
C(1)	180	3.775	7	0.02	0.0
C(2)	180	3.778	7	0.02	+0.1
D	270	3.787	7	0.03	+0.3

Pooled Mean:

[A(1) + A(2) + A(3) + A(4)]/4 = 3.756 x 10^{-6} ohm

B = 3.780

[C(1) = C(2)]/2 = 3.777

D = 3.787

15.100 Sum

Pooled Mean = [15.100/4] = 3.775 x 10^{-6} ohm

A	0	3.780	5	0.01	-0.18
B	90	3.791	5	0.01	+0.11
C	180	3.794	5	0.06	+0.20
D	270	3.781	5	0.02	-0.13

Mean = 3.787 x 10^{-6} ohm

Grand Mean = 3.78 x 10^{-6} ohm

Table 8. Measurement results for a 2.5-cm diameter fixed Rogowski coil.

Test Position Designation	Coil Position Rotation (degrees)	Coil/Amplifier Transimpedance (x 10^{-6} ohm)	No. of Meas.	Std. Dev. ±(%)	Diff. from Mean (%)
A(1)	0	35.467	7	0.02	-1.2
A(2)	0	35.479	7	0.02	-1.1
B(1)	90	35.813	7	0.02	+0.2
B(2)	90	36.005	7	0.02	+0.3
C	180	36.496	7	0.02	+1.7
D(1)	270	36.416	7	0.03	+1.5
D(2)	270	36.485	7	0.02	+1.7

Pooled Mean:

$[A(1) + A(2)]/2 = 35.473 \times 10^{-6}$ ohm
$[B(1) + b(2)]/2 = 35.909$
$C = 36.496$
$[D(1) + D(2)]/2 = 36.451$
144.329 Sum

Pooled Mean = $[144.329/4] = 36.1 \times 10^{-6}$ ohm

E	---	35.258	7	0.02	-1.8

3.3.4 Summary of Test Results for Rogowski Coils

Several conclusions can be drawn from the results of testing three Rogowski current sensing coils using the methods discussed herein. One surprising fact was that repeatable data can be obtained in any one data set providing that the coil being tested is not moved or repositioned. This is true even if there are significant nonlinearities in the field being sensed. It also means that the field "shape" was constant during the tests. Standard deviations of 5 to 7 repeated measurements consistently were less than ±0.05%. Whenever the standard deviation was greater than ±0.1%, there was generally a problem in calculations or some experimental error.

The split-type of Rogowski coils have significantly more rotational sensitivity than the fixed-type. The measurements performed above support this conclusion that was also reached by previous measurements [2]. It is apparent that larger measurement errors can result for such coils when the field is severely nonlinear, such as when the return current conductor is near the coil. This is the case for all of the tests performed above. There were no apparent temperature related problems when performing measurements on any of the coils.

3.4 Estimates of Measurement Uncertainties

Measurement uncertainties may arise from many sources in the process of calibrating current sensors such as high-current shunts or Rogowski coils. Certainly, factors such as the stability and linearity of the sensors are important, and for measurements at the low-end of their operating ranges, noise can become a contributing factor. Extraneous effects such as induced voltages in signal leads or ground loops offer still more complications in estimating uncertainties. All the major factors have been taken into account and the estimate should be sufficiently conservative to encompass the range of real uncertainties. These estimates will decrease as the measurement process is refined, and as system components are upgraded. The manner in which the individual uncertainties are combined is an arbitrary choice that seems to "fit the model" for the process.

Uncertainty estimates are given below for measurements of both shunts and Rogowski coil sensors.

MEASUREMENT UNCERTAINTIES

Voltage Measurement (per channel):		
Digitizing resolution (± 1/2 LSB)	±0.10%	FS Range
Linearity	±0.17%	
Ranging and Gain	±0.22%	
Noise	±0.008%	
	±0.50%	Sum
NBS Reference Standard Mutual Inductor:		
Calibration Constant	±0.03%	
Nonlinearity and Positional Sensitivity	±0.05%	
Noise, Misc	±0.02%	
	±0.10%	Sum
Randomness (3 standard deviations):		
Shunt measurements	±0.15%	max
Rogowski coil measurements	±0.15%	max

In addition to the above measurement uncertainties, the effects listed below must be included into the estimate for the overall uncertainty to which a shunt or Rogowski coil can be realistically calibrated.

MISCELLANEOUS EFFECTS

Shunt:		
Temperature effects (for a 10°C rise)	±0.15%	
Positional sensitivity	±0.10%	
Noise and induced voltages, ground loops, proximity effects, etc.	±0.30%	
	±0.55%	Sum
Rogowski Coils (with integrating amplifier):		
Linearity	±0.10%	

Noise, hum, induced voltages, ground loops, etc. ..... ±0.10%

Positional sensitivity:

12.7-cm split coil ..... ±10.0%

6.4-cm fixed coil ..... ±1.5%

2.5-cm split coil ..... ±2.0%

12.7-cm split coil ±10.2% Sum

6.4-cm fixed coil ±1.7% Sum

2.5-cm split coil ±2.2% Sum

OVERALL COMBINED UNCERTAINTY FOR CALIBRATION OF:

Shunt:

Sum of effects listed above ..... ±0.55%

Voltage measurements (channel one) ..... ±0.50%

(channel two) ..... ±0.50%

NBS reference standard ..... ±0.10%

Computation errors, rounding, etc. ..... ±0.10%

Randomness ..... ±0.15%

$0.55 + [0.5^2 + 0.5^2 + 0.1^2 + 0.1^2 + 0.15^2]^{1/2} = \pm 1.27\%$ rss

12.7-cm Split Coil:

Sum of effects listed above ..... ±10.2%

Voltage measurements (channel one).. ±0.50%

(channel two).. ±0.50%

NBS reference standard ..... ±0.10%

Computation errors ..... ±0.10%

Randomness ..... ±0.15%

$10.2 + [0.5^2 + 0.5^2 + 0.1^2 + 0.1^2 + 0.15^2]^{1/2} = \pm 10.9\%$ rss

6.4-cm Fixed Coil:

Sum of effects listed above ..... ±1.7%

Voltage measurements (channel one) .. ±0.50%

(channel two) .. ±0.50%

NBS reference standard ..... ±0.10%

Computation errors ..... ±0.10%

Randomness ..... ±0.15%

$1.7 + [0.5^2 + 0.5^2 + 0.1^2 + 0.1^2 + 0.15^2]^{1/2} = \pm 2.44\%$ rss

2.5-cm Split Coil:

Sum of effects listed above ..... ±2.2%

Voltage measurements (channel one) .. ±0.50%

(channel two) .. ±0.50%

NBS reference standard ..... ±0.10%

Computation errors ..... ±0.10%

Randomness ..... ±0.15%

$2.2 + [0.5^2 + 0.5^2 + 0.1^2 + 0.1^2 + 0.15^2]^{1/2} = \pm 2.94\%$ rss

Table 9 gives the transimpedances of the sensors tested and estimated uncertainties for the values reported.

Table 9. Shunt and Rogowski coil and integrating amplifer transimpedances and estimated uncertainties.

Sensor Designation	Sensor Transimpedance (x 10^{-6} ohm)	Estimated Uncertainty ±(%)
30-kA Shunt	10.06	1.27
12.7-cm split coil	3.74	10.9
6.4-cm fixed coil	3.78	2.4
2.5-cm split coil	36.1	2.9

4. SAFETY CONSIDERATIONS

Safety considerations were briefly investigated relating to the operation and use of the 100-kA source for the calibration and evaluation of high-current sensors. There are three main areas of concern which are:

- o High-voltage hazards
  - Primary circuits
  - Secondary circuits
- o High secondary currents
  - Magnetic fields
  - Heating effects
- o Mechanical considerations

High-Voltage Hazards: There are definite life-threatening hazards due to the presence of high ac voltages used in the operation of the current source. The source is fed from 480-V single-phase power lines that are fused for 500 A and capable of delivering surge currents in excess of several thousand amperes for short periods of time before fuses open. In addition to the direct electrical shock dangers, there are burn hazards should a conductor (such as a tool like a screwdriver, for example) cause an inadvertant short. The flash and possible spraying of molten metals could cause serious burns.

Most of the 480-V circuitry is interlocked to prevent accidental exposure to the live portions of the equipment. The areas in which the

autotransformers are located is normally enclosed and cannot be accessed without removing a panel. If access is required, the main double-pole disconnect is opened removing all voltage from the system. In instances when it is necessary to work on the system while energized in the presence of the primary voltage, a second person should always be present.

In normal use and without failure of hardware such as the 250-kVA output transformer, the maximum secondary voltage is not greater than 14.2 V rms and presents no shock hazard. There is always a remote chance that the output transformer could short from the primary to the secondary in such a way that the primary voltage could be placed onto the secondary. When possible, one side of the secondary circuit is connected to an earth ground. In some instances, this cannot be done because of "double-grounding" conditions when shunts are being used and are grounded through the instrumentation. In the latter instance, the instrument ground provides some protection. The transformer manufacturer stated that primary-to-secondary shorts are extremely rare, and the only times they had ever observed this to happen was when the transformer had been abused and overheated for long periods of time. Saturable reactors can be used across the secondary, or from each side of the secondary to ground to add protection. The addition of such a device is being planned though it may interfere with the accuracy with which shunts can be calibrated.

There is sufficient electrical capacitance between the primary and secondary windings of the output transformer that a charge can build up or be coupled onto the secondary bus-bars. This is not considered lethal, but the voltage can be high enough so that one can get shocked and startled. The physical reaction of this light shock could cause damage by striking some object while trying to "escape" from the bus-bar. Temporarily grounding the bus just before making contact will minimize this hazard. (In one instance, this charge was sufficient to damage the input to the digitizer when a shunt was being connected.)

High Secondary Currents: The ac-magnetic fields created by the high currents can be quite large very near the secondary bus-bars, especially if a loop is formed. In the region of a loop, magnetic field strengths greater than 0.01 T peak may exist at full output currents. In normal use of the current source, the operator is at least one meter removed from the vicinity of the bus bars. Field measurements that were made indicated that the ac-magnetic field strength was less than 205 μT peak at that distance at a full output current of 100 kA peak, and thus is considered biologically harmless.

One hazard from high currents comes from the possibility that a loose connection could "sputter", thus spraying molten metals at the operator causing burns, or starting a fire. This problem is minimized when using conductors properly sized for the currents, and when all electrical connections are tight and of low impedance. The experience of welding equipment manufacturers and users suggests that there is a minimal hazard if there is a loose or poor connection. High impedance limits sufficient currents from flowing that could cause "sputtering".

When using heavy flexible cables in the secondary, there is a tendency for the conductors to whip or flail, especially at higher currents. All such cables MUST be secured and positioned such that motion is minimized. High ac-

magnetic fields, though not viewed as a biological hazard, might cause serious damage to data stored on magnetic storage media such as tapes or floppy disks. These data storage media should be kept at least several meters away from the current source.

Mechanical Hazards: The only serious mechanical hazards of concern are those related with lifting and positioning heavy copper bus bars. For those pieces too large for one person to handle, a second person is needed. If it is necessary to move larger parts into position, then mechanical assistance is used. Care must be exercised to minimize the hazard of dropping heavy bus-bar parts on one's foot.

5. FUTURE EFFORTS AND RECOMMENDATIONS

The near-term effort for additional work on this project includes, but is not limited to, performing field (on-site) measurements; that is, performing shunt and Rogowoski coil calibrations on welding systems being used in the field. This is needed to discover the real problems that might be encountered and to assess the typical measurement uncertainties that can be expected. Several sites have been suggested and it is expected that measurements will be made at each within the next one- to two-year period.

There is still much to be learned about the performance of shunts and Rogowski coils used to measure high currents. Calibration procedures are expected to evolve once the major problems are understood. Laboratory investigation will continue regarding the performance and characteristics of shunts and Rogowski coils. This includes the development of methods to measure the outputs of shunts which are used in grounded bus-bar arrangements. Other sensors, such as opto-electronic sensors will be investigated as they become available.

Recommendations include the following:

- Incorporate a better digitizer into the measurement system. The present 10-bit analog-to-digital converters are barely adequate. It is recommended that 12- or 14-bit converters be used.

- Incorporate a faster analyzer into the measurement process. The present digital analyzer is slow in performing such operations as determining the rms values of digitized waveforms. Because much of this must be done, speeding this process will save significant laboratory time.

- Incorporate a dual floppy disk drive into the data gathering system to provide an effective means for storing waveforms and data analysis results. The double drive would make system operations go faster and provide a means for backing up valuable data disks.

- Design, fabricate, and test a coaxial "current cage" so that testing of coils and shunts could be done in an environment of low axial and radial magnetic fields.

- Continue to search for, or design and fabricate, better Rogowski coils that have significantly less positional sensitivity than those tested thus far.

6. CONCLUSIONS

The characterization of a 100-kA pulsed current source was performed. The system configuration and operation were described. The output current limits were established as approximately 103 kA peak for heat settings of 99% and for durations of 8-cycles of a 60-Hz sinusoidal waveform. The output current levels as a function of the heat settings were determined. The maximum levels are set by fusing limits, while the minimum levels are set by the minimum voltages necessary for proper SCR operation. Generally, current levels of less than about 6 kA rms at 99% heat are unachievable with this system as presently configured.

The current waveform and spectra were examined. As the heat settings decrease, the amount of harmonic content increases. The odd harmonics were present and decreased with an increase of harmonic order. No significant content was observed at frequencies greater than about 1 kHz.

The magnetic field strength in a near field was measured and plotted. Although this will change with each bus-bar configuration, the near field (within 25 cm of the bus-bar) was measured to be less than 2000 μT rms for secondary currents of 16 kA rms. At distances greater than 1 m, the magnetic field strength was considerably less than 100 μT rms.

Shunt and Rogowski coil current sensor calibration procedures and philosophy were discussed. The digitization and necessary mathematical operations were described. Calibration results for several 30 000-A shunts and several Rogowski coil current sensors were given. A heating effect was noted while calibrating the shunts and is believed to be related to thermally induced strain. The calibration of the Rogowski coils was necessary at several rotational positions because of their sensitivity to nonuniform fields. The split-type coils in all instances showed more error due to position than did the fixed type coil. If the coil's position is not disturbed during a calibration sequence, repeatability (one standard deviation) can generally be expected to be better than 0.05%. Overall uncertainties of shunt and coil calibrations range from about 1.3% to 11%, depending on factors such as heating, in the case of shunts, or position in the case of coils.

7. ACKNOWLEDGEMENTS

This project was sponsored by the Sandia National Laboratories, Albuquerque, New Mexico. Mr. S.R. Booker, of that laboratory has made many constructive comments and stimulated thinking regarding the problems of these and related measurements. The current source was designed, built, and delivered by the Sandia National Laboratories at Livermore, California. Mr. J. Hopwood provided instruction regarding the operation of the system and assisted in assessing the maximum current capabilities of the source. The author expresses appreciation to these and others who have contributed to this effort. Thanks also are due to Mrs. Karen Heilers and Mrs. Roberta Cummings who prepared this manuscript.

8. REFERENCES

1. W. F. Praeg, Low-Inductance Shunts for Measuring Large Pulsed Currents, Nat. Bur. Stand. (U.S.), Special Publication 628, Measurement of Electrical Quantities in Pulse Power Systems, R. H. McKnight and R. E. Hebner, eds., June, 1982.

2. J. D. Ramboz, and D. R. Flach, High-Current Measurement Techniques, Nat. Bur. Stand. Report NBSIR 84-2881, May 1984.

NBS-114A (REV. 2-8C)

U.S. DEPT. OF COMM. BIBLIOGRAPHIC DATA SHEET (See instructions)	1. PUBLICATION OR REPORT NO. NISTIR 89-4040	2. Performing Organ. Report No.	3. Publication Date MARCH 1989

4. TITLE AND SUBTITLE

HIGH-CURRENT MEASUREMENT TECHNIQUES, PART II
100-kA SOURCE CHARACTERISTICS AND PRELIMINARY SHUNT AND ROGOWSKI COIL EVALUATIONS

5. AUTHOR(S)

J. D. Ramboz

6. PERFORMING ORGANIZATION (If joint or other than NBS, see instructions)

NATIONAL BUREAU OF STANDARDS
U.S. DEPARTMENT OF COMMERCE
GAITHERSBURG, MD 20899

7. Contract/Grant No.

8. Type of Report & Period Covered

9. SPONSORING ORGANIZATION NAME AND COMPLETE ADDRESS (Street, City, State, ZIP)

Sandia National Laboratories, Albuquerque, New Mexico, 87185

10. SUPPLEMENTARY NOTES

☐ Document describes a computer program; SF-185, FIPS Software Summary, is attached.

11. ABSTRACT (A 200-word or less factual summary of most significant information. If document includes a significant bibliography or literature survey, mention it here)

The characterization of a 100-kA current source is discussed. This source is intended for use in the calibration of high-current sensors such as shunts and Rogowski coils commonly employed in resistance welders. The output current from the source is derived from SCR-gated signals in the form of bursts of "chopped" 60-Hz sinsusoidal waveforms. These waveforms and their spectral content were investigated. The near-field magnetic field strength was mapped. Initial calibrations were performed on a 30-kA, 10-μΩ shunt. Preliminary results indicate a temperature coefficient of about 130 ppm/°C which is thought to be related to a thermally induced strain. Several Rogowski coil type current sensors were evaluated and calibrated. Each of the coils measured had outputs which were sensitive to the rotational position about the current carrying conductor. The calibration philosophy and approach is discussed and estimates of measurement uncertainty are given. Suggested improvements for the measurement process are offered. Planned efforts are outlined.

12. KEY WORDS (Six to twelve entries; alphabetical order; capitalize only proper names; and separate key words by semicolons)

ac current measurements; ac current shunts; calibration; high-current generation; high-current measurements; Rogowski coils

13. AVAILABILITY

☒ Unlimited

☐ For Official Distribution. Do Not Release to NTIS

☐ Order From Superintendent of Documents, U.S. Government Printing Office, Washington, D.C. 20402.

☒ Order From National Technical Information Service (NTIS), Springfield, VA. 22161

14. NO. OF PRINTED PAGES

51

15. Price

$14.95